# Model based analysis of lateral and vertical soil carbon fluxes induced by soil redistribution processes in a small agricultural catchment

**Verena Dlugoß, Peter Fiener, Kristof Van Oost, Karl Schneider**

**Angaben zur Veröffentlichung / Publication details:**

Dlugoß, Verena, Peter Fiener, Kristof Van Oost, and Karl Schneider. 2012. "Model based analysis of lateral and vertical soil carbon fluxes induced by soil redistribution processes in a small agricultural catchment." *Earth Surface Processes and Landforms* 37 (2): 193–208. https://doi.org/10.1002/esp.2246.



# Model based analysis of lateral and vertical soil carbon fluxes induced by soil redistribution processes in a small agricultural catchment

**Verena Dlugoß,[1] Peter Fiener,[1,2]* Kristof Van Oost[3] and Karl Schneider[1]**

[1] Department of Geography, University of Cologne, Cologne, Germany

[2] Indo-German Centre for Sustainability, Indian Institute of Technology Madras, Chennai, India

[3] Earth and Life Institute, Georges Lemaître Centre for Earth and Climate Research (TECLIM), Université catholique de Louvain, Louvain-la-Neuve, Belgium

*Correspondence to: Peter Fiener, Department of Geography, University of Cologne, Albertus Magnus Platz, 50923 Cologne, Germany. E-mail: peter.fiener@uni-koeln.de

ABSTRACT: Soil redistribution on arable land significantly affects lateral and vertical soil carbon (C) fluxes (caused by C formation and mineralization) and soil organic carbon (SOC) stocks. Whether this serves as a (C) sink or source to the atmosphere is a controversial issue. In this study, the SPEROS-C model was modified to analyse erosion induced lateral and vertical soil C fluxes and their effects upon SOC stocks in a small agricultural catchment (4·2 ha). The model was applied for the period between 1950 and 2007 covering 30 years of conventional tillage (1950–1979) followed by 28 years of conservation tillage (1980–2007). In general, modelled and measured SOC stocks are in good agreement for three observed soil layers. The overall balance (1950–2007) of erosion induced lateral and vertical C fluxes results in a C loss of $-4{\cdot}4\,\mathrm{g\,C\,m^{-2}\,a^{-1}}$ at our test site. Land management has a significant impact on the erosion induced C fluxes, leading to a predominance of lateral C export under conventional and of vertical C exchange between soil and atmosphere under conservation agriculture. Overall, the application of the soil conservation practices, with enhanced C inputs by cover crops and decreased erosion, significantly reduced the modelled erosion induced C loss of the test site. Increasing C inputs alone, without a reduction of erosion rates, did not result in a reduction of erosion induced C losses. Moreover, our results show that the potential erosion induced C loss is very sensitive to the representation of erosion rates (long-term steady state versus event driven). A first estimate suggests that C losses are very sensitive to magnitude and frequency of erosion events. If long-term averages are dominated by large magnitude events modelled erosion induced C losses in the catchment were significantly reduced. 

KEYWORDS: soil erosion; soil carbon; modeling; soil conservation

## Introduction

In current global and regional climate change research, the role of soil organic carbon (SOC) and its vertical and lateral fluxes have become an important issue (e.g. Ciais *et al.*, 2010). The pedosphere is the world's third largest carbon (C) pool, and soil and climate systems are closely linked by the exchange of C between the atmosphere, biosphere, and pedosphere (Schlesinger, 2005). Globally, vast quantities of this SOC pool ($0{\cdot}47$ to $0{\cdot}61\,\mathrm{Pg\,a^{-1}}$) are moved laterally across the earth surface as a result of agricultural soil erosion (Van Oost *et al.*, 2007). However, the impact of soil erosion on the vertical C flux (net effect of SOC formation and mineralization) and whether soil redistribution on agricultural land constitutes a C sink or source to the atmosphere is less clear. Estimations of the carbon dioxide ($CO_2$) sink/source strength caused by soil erosion and deposition range from a source of $0{\cdot}8$ to $1{\cdot}2$ Pg C per year (Lal, 2003) to a sink of $0{\cdot}12$ to $1{\cdot}5$ Pg C per year (Stallard, 1998; Smith *et al.*, 2001; Renwick *et al.*, 2004; Van Oost *et al.*, 2007). Van Oost *et al.* (2007) identified three key mechanisms related to erosion processes that affect the net C flux between pedosphere and atmosphere of eroding croplands. These mechanisms are: (i) the (partial) C-replacement of eroded SOC at sites of erosion (Harden *et al.*, 1999) resulting from continued C input by plants combined with a decreased decomposition due to a decrease in SOC content; (ii) the burial of SOC in low mineralization contexts such as depositional sites (Smith *et al.*, 2001, 2005); and (iii) the enhanced decomposition of SOC during detachment and transport of soil particles due to the breakdown of stabilizing aggregates (Lal, 2003). The highly variable global estimates of the net C flux result from different assumptions referring to these mechanisms and their balance as well as from different estimates of global soil erosion rates (Billings *et al.*, 2010).

These large uncertainties highlight the need for further investigations especially at the catchment scale, where different landscape elements are integrated into one geomorphic system. As SOC stocks and soil-atmosphere C fluxes are highly spatially variable (e.g. Ritchie *et al.*, 2007; Dlugoß *et al.*, 2010), the use of a coupled and spatially explicit SOC and soil redistribution

model is a useful tool to analyse SOC dynamics and its interplay with soil redistribution at the catchment scale (Polyakov and Lal, 2004; Van Oost *et al.*, 2005a; Yadav and Malanson, 2009).

Several approaches of integrated models of erosion processes and C cycling have been presented in the literature. Reviews are given in Polyakov and Lal (2004) and in Van Oost *et al.* (2009). These approaches are often restricted to single points at different landscape positions using erosion and/or deposition rates derived from measurement or modelling (Gregorich *et al.*, 1998; Harden *et al.*, 1999; Pennock and Frick, 2001). The simulation of soil C dynamics in these studies relies on the CENTURY (Parton *et al.*, 1987) SOC model that was restricted to the simulation of one soil layer in its early version. Liu *et al.* (2003) used a modified version of CENTURY, the EDCM (Erosion-Deposition-Carbon-Model), and Billings *et al.* (2010) developed the spread-sheet model SOrCERO (Soil Organic Carbon, Erosion, Replacement, and Oxidation), both allowing for the simulation of several soil layers. But in these studies the models were also applied to single soil profiles at different slope positions.

Recently, models allowing for an improved integrated spatial analysis of the impact of soil redistribution on SOC dynamics at the catchment scale have been developed by combining spatially explicit geomorphic models, including soil redistribution, with models of soil C dynamics (Rosenbloom *et al.*, 2001; Yoo *et al.*, 2005; Van Oost *et al.*, 2005a; Yadav and Malanson, 2009)\. The Changing Relief and Evolving Ecosystems Project (CREEP) (Rosenbloom *et al.*, 2001) and the model presented by Yoo *et al.* (2005) simulate diffusive geomorphic processes on undisturbed grasslands and focus on the long-term hillslope response. In contrast, SPEROS-C (Van Oost *et al.*, 2005a) and the combined CENTURY and GeoWEPP (Renschler, 2003) model presented by Yadav and Malanson (2009) focus on contemporary geomorphic processes occurring on arable land. Both models consider different soil layers and explicitly simulate changing controls on C input and decomposition with depth.

To our knowledge, the only model that also considers soil redistribution induced by tillage operations, a phenomenon that has been recognized in soil erosion research since the 1990s (e.g. Lindstrom *et al.*, 1992; Govers *et al.*, 1994), is the model SPEROS-C (Van Oost *et al.*, 2005a), which combines the Introductory Carbon Balance Model (ICBM, Andrén and Kätterer, 1997) with the soil erosion model SPEROS (Van Oost *et al.*, 2003). On sloping arable fields, tillage induced erosion and deposition can be more important than erosion processes associated with water (e.g. Van Oost *et al.*, 2005a). In addition, tillage erosion significantly changes soil redistribution patterns (Govers *et al.*, 1994), thus making a consideration of tillage erosion necessary. Since previous studies proved the suitability of SPEROS-C to simulate SOC dynamics for the last 50 years in small (~4 ha) agricultural catchments under conventional tillage in Denmark and Great Britain (Van Oost *et al.*, 2005a), we chose this model for our study. In our test site, a change of land management occurred in the 1980s, providing the opportunity to analyse the interaction of soil redistribution and SOC dynamics introduced by changes in land management. Although land management is known to have a large effect on both SOC stocks (e.g. Gregorich *et al.*, 1998; Eynard *et al.*, 2005; Jarecki *et al.*, 2005) and soil erosion rates, expressed, e.g. in the crop management factor of the Universal Soil Loss Equation (USLE) (Wischmeier and Smith, 1978), on arable land, these processes are mostly studied in isolation.

Against this background, the objectives of our study are (i) to modify the SPEROS-C model in order to analyse the effects of soil redistribution on lateral sediment-burden SOC fluxes and vertical C fluxes between soil and atmosphere in a small arable catchment in Germany, (ii) to explore the integrated effect of changes in land management on soil redistribution and on the soil C balance, and (ii) to investigate the sensitivity of the simulated C fluxes to uncertainties in model inputs.

## Materials and Methods

### Test site

The Heiderhof test site is located in the Pleiser Hügelland, a hilly landscape about 30 km southeast of Cologne in North Rhine-Westphalia, Germany. It is a small arable catchment of 4·2 ha (part of a larger field; altitude 125–154 m above sea level (a.s.l.); 50°43′N, 7°12′E). Slopes range from 1° in the west up to 9° in the east with a relatively flat thalweg area heading to the outlet (Figure 1). Due to its fertile, silty and silty-loamy soils (mean sand, silt and clay content of 13%, 68% and 19%, respectively), classified as Luvisols (FAO, 1998), the test site has a long history of arable land use (Preston, 2001). The crop rotation has consisted of sugar beet (*Beta vulgaris* L.), winter wheat (*Triticum aestivum* L.), and winter barley (*Hordeum vulgare* L.) since the 1950s. Until 1980, the test site was tilled by mouldboard ploughing with a tillage depth of 0·25 m. Since 1980, a conservation tillage system has been established with chisel instead of mouldboard ploughing (tillage depth 0·15 m) and mustard (*Sinapis arvensis* L.) cultivated as a cover crop after winter barley.

The Heiderhof test site is part of the Dissenbach catchment (~150 ha), where runoff, sediment and C delivery have been monitored since 2006. Land use in the Dissenbach catchment is representative for this intensively used area close to the agglomeration of Cologne-Bonn. Approximately 70% of the area, especially the moderate slopes, is used for arable agriculture, while the flat and wetter areas along the Dissenbach are used as grassland (~15% of the catchment area).

The mean annual air temperature is 10·0 °C and the average annual precipitation is 765 mm (1990–2006) with the highest rainfall intensities occurring from May to October (data from the German Weather Service station Bonn-Roleber, situated about 1 km to the west of the test site, 159 m a.s.l.).

### Field measurements

#### Soil redistribution estimate

Radiogenic nuclides, especially caesium-137 ($^{137}$Cs), are often used to derive spatially distributed time-integrating soil erosion and deposition rates (e.g. Walling *et al.*, 2003; Li *et al.*, 2010). At our test site, $^{137}$Cs measurements (GSF, Neuherberg, Germany) indicate a contamination due to nuclear weapon testing in the 1950s and 1960s as well as to fallout following the Chernobyl disaster in 1986. However, as the intensity of $^{137}$Cs contamination in both periods is unknown, and as the Chernobyl $^{137}$Cs was potentially deposited during a limited number of heavy rainfall events causing spatially heterogeneous deposition by surface runoff, it is not possible to use $^{137}$Cs as a tracer of soil erosion at the test site.

Since alternative tracers encompassing a time period of roughly 50 years are hardly available, we used carbon-14 ($^{14}$C) AMS (accelerator mass spectrometry) data as a qualitative indicator of soil deposition since the 1950s. Due to nuclear weapon testing, the atmospheric $^{14}$C content has increased significantly since the 1950s with a peak in 1963 (~180 pMC) that was almost double the atmospheric $^{14}$C content of the period before 1950 (97·5 pMC) (Levin and Kromer, 2004). In 2009, when our soil samples were taken, the atmospheric

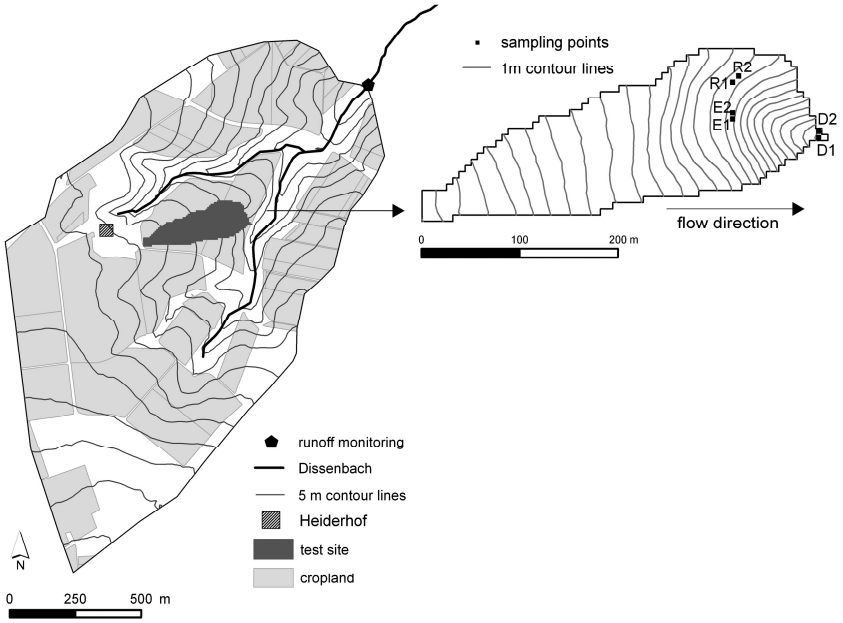


**Figure 1.** Location and topography of the test site within the Dissenbach catchment, where runoff, sediment and carbon delivery are measured at a San Dimas flume. Sampling points are located at reference (R), depositional (D) and erosional (E) sites.

$^{14}$C content of 104·7 pMC was still slightly higher than the value before 1950. This so-called bomb spike can be used as a time marker to study SOC dynamics on decadal timescales (Trumbore, 2009).

To qualitatively estimate deposition in our test site, two soil profiles each were selected at a depositional, erosional, and a reference site (ignorable erosion or deposition) (Figure 1). At the depositional site, soil cores were taken up to 1·6 m in depth, whereas sampling depth at the reference and the erosional sites was 1·2 m and 0·8 m, respectively. Except for the uppermost 0·15 m, being the actual tillage depth, soil cores were divided into 5 cm increments. The $^{14}$C content of bulk soil samples of every second increment starting with the topsoil layer was measured at the AMS facility of the Institute of Particle Physics of the Swiss Federal Institute of Technology, Zurich, Switzerland. The $^{14}$C concentrations were calculated from the measured $^{14}$C/$^{12}$C ratio of the sample compared to 95% of the NIST oxalic acid standard (NIST, National Institute of Standards and Technology, Gaithersburg, USA), both corrected for isotopic fractionation using the simultaneously measured $^{13}$C/$^{12}$C ratio. Data are expressed according to Stuiver and Polach (1977) in percent modern carbon (pMC; 100 pMC = 1950).

For a simple estimate of deposition, we assumed that the $^{14}$C content of bulk soil in the plough layer is represented by the atmospheric $^{14}$C content due to a large fraction of recent soil organic matter (Rethemeyer *et al.*, 2005) and that the $^{14}$C content of buried material at depositional sites is stable. Thus, using bomb $^{14}$C as a tracer of topsoil, we expected an increase of $^{14}$C with increasing soil depth at the depositional site due to the burial of SOC imprinted by bomb-$^{14}$C since 1950, whose extention in depth corresponds to the deposition height since 1950. This increase was expected to have a similar shape as the developing of the atmospheric $^{14}$C concentration, being more or less attenuated depending on the turnover rate of the buried C. The simplest estimate of deposition is to derive the depth increment when $^{14}$C contents start to fall below the values attributed to the bomb-$^{14}$C curve, assuming that this material is older than 1950. In a more complex approach, we reconstructed the depth development of $^{14}$C at the depositional site using the bomb C turnover model of Harkness *et al.* (1986). Assuming no other forms of soil mixing, loss of radiocarbon at erosion sites proportional to the mean modelled erosion rate and a gain of radiocarbon at deposition sites proportional to the modelled deposition rate were integrated into this model. The eroded radiocarbon from the plough layer at the erosional site is transferred to the plough layer at the depositional site, where the actual plough layer is buried deeper in the soil profile. The eroded fraction from the plough layer at the erosion site is replaced by the corresponding amount from the subsoil.

Following this, the $^{14}$C activity at time $t$ of bulk SOC in the plough layer at erosional sites $A_{t/Epl}$ (in pMC) is calculated as

$$A_{t/Epl} = \left[A_{(t-1/Epl)} \cdot e^{-k} + A_i \cdot (1 - e^{-k}) - A_{(t-1/Epl)} \cdot \lambda\right] \cdot (1 - f_E) + A_{sub} \cdot f_E \quad (1)$$

and for the plough layer at depositional sites $A_{t/Dpl}$ (in pMC) it is calculated as

$$A_{t/Dpl} = \left[A_{(t-1/Dpl)} \cdot e^{-k} + A_i \cdot (1 - e^{-k}) - A_{(t-1/Dpl)} \cdot \lambda\right] \cdot (1 - f_D) + A_{t/Epl} \cdot f_D \quad (2)$$

respectively. For the buried plough layer at depositional sites, the $^{14}$C activity $A_{t/Dbur}$ is calculated as

$$A_{t/Dbur} = A_{(t-1/Dpl)} \cdot e^{-k} + A_i \cdot (1 - e^{-k}) - A_{(t-1/Dpl)} \cdot \lambda \quad (3)$$

$A_{(t-1/Epl,\ Dpl)}$ is the $^{14}$C activity in the plough layer at erosion and depositional sites of the previous year (in pMC), $A_i$ is the input $^{14}$C activity of plant residue corresponding to the atmospheric $^{14}$C activity for agricultural plants (in pMC), $A_{sub}$ is a constant $^{14}$C activity assumed for bulk SOC in the subsoil (in pMC), $k$ the SOC turnover rate (in a$^{-1}$) and $\lambda$ the $^{14}$C decay constant (1/8268 a$^{-1}$). The variables $f_E$ and $f_D$ represent the fraction of eroded/deposited soil of the plough layer. Different erosion rates (0·1, 1, and 2 mm a$^{-1}$) are applied to account for differences in the origin and hence $^{14}$C depletion of the deposited soil. The SOC turnover rate $k$ is set to 0·006 corresponding to the passive pool of SPEROS-C (Van Oost *et al.*, 2005a) and is assumed to remain stable with depth and slope position. The $^{14}$C activity of the subsoil is set to 80 pMC as derived from measurements on undisturbed sites by Rethemeyer *et al.*

(2005). Atmospheric $^{14}C$ concentrations are derived from Levin and Kromer (2004). The deposition rate was then iteratively adjusted so that the reconstructed $^{14}C$ depth distribution qualitatively fitted the measured one.

Additionally, SOC and soil texture were determined for the chosen soil samples. SOC content was measured by dry combustion using a CNS elemental analyser (VarioEL, Elementar, Hanau, Germany), and soil texture was derived by the combined sieve and pipette method (Deutsches Institut für Normung, 2002).

### Spatially distributed soil properties

In 2006 and 2007, an intensive soil sampling campaign was carried out in the test site and soil samples were taken in a regular 17 m by 17 m grid ($n = 144$) at three depths (I: 0–0·25; II: 0·25–0·50 m; III: 0·50–0·90 m) (Dlugoß *et al.*, 2010). For each of these samples, SOC as well as soil texture were determined as described earlier, while soil bulk density was determined on 15 of these sampling points by weighing the soil samples after oven drying at 105 °C (volumetric core method).

The measured SOC data were interpolated to a 6.25 m × 6.25 m grid ($n = 1030$) by means of geostatistics for each soil layer (Dlugoß *et al.*, 2010). In each layer, the best interpolation result (produced by ordinary kriging in soil layer I and by regression kriging in layers II and III, respectively) was taken as validation data for the modelled SOC distributions. Soil texture and soil bulk density data were used for model implementation.

### Runoff, sediment and carbon delivery

In March 2006, a San Dimas flume (Kilpatrick and Schneider, 1983; Grant and Dawson, 1997) was installed at the outlet of the Dissenbach catchment (Figure 1). Here, precipitation and water-level are measured continuously, and runoff is derived by a calibrated stage-discharge equation (Kilpatrick and Schneider, 1983; Grant and Dawson, 1997). An automatic sampler (AWS, EcoTech, Bonn, Germany) continuously takes water samples once a day as well as event-driven samples, i.e. when a critical water-level, which varies seasonally, is exceeded. The sediment content of the sampled water is determined by filling two aliquots of 100 ml into beakers after carefully shaking the sample bottles for two minutes. The samples are then oven-dried at 105 °C and weighed. If sediment content is approximately $> 2\ g\ l^{-1}$, its SOC content is determined by dry combustion using a CNS elemental analyser (Elementar, Hanau, Germany).

Based on these sediment and SOC samples, the sediment and C delivery of the Dissenbach catchment was calculated for the years 2007 to 2009. However, it must be noted that SOC delivery could only be determined for large erosion events constituting ~35% of the total sediment yield in 2007 and 2008 and ~54% in 2009, respectively. Hence, we estimated total SOC delivery assuming that the average C content in sediment during large events can be applied to total sediment output, even if this seems to be a conservative estimate (Wang *et al.*, 2010). Based on these data, the average enrichment of C in sediments, as compared to the parent soil material, was calculated using topsoil SOC information from the entire Dissenbach catchment derived from a digital soil map provided by the Geological Survey of North-Rhine Westphalia.

The data measured at the Dissenbach outlet were used to analyse the results from erosion and SOC modelling at the Heiderhof sub-catchment. The focus was the comparison of the overall erosion on both scales and especially to the enrichment of C in delivered sediment.

## Model description SPEROS-C

### Soil redistribution

The soil redistribution component of SPEROS-C consists of a water and a tillage erosion component that can be run separately. In order to apply the model at our study site, we replaced the calculation of potential water erosion with those of the WaTEM model (Van Oost *et al.*, 2000; Van Rompaey *et al.*, 2001). The Revised Universal Soil Loss Equation (RUSLE)-type erosion component allows (i) to account for a change in land management during the simulation period, and (ii) to avoid a site-specific calibration necessary for the original water erosion component (Van Oost *et al.*, 2003, 2005a) since the use of tracer data like $^{137}Cs$ was not possible in our test site.

To apply the RUSLE in a two-dimensional landscape, the slope length factor was replaced in WaTEM/SEDEM using the unit contributing area following Desmet and Govers (1996a). To account for sediment transport and deposition, sediment transport is calculated using the flux decomposition approach by Desmet and Govers (1996b), while deposition is controlled by the local transport capacity $TC$ (in $kg\ m^{-1}\ a^{-1}$) calculated for each grid cell following Verstraeten *et al.* (2006):

$$TC = ktc \cdot R \cdot K \cdot (LS - 4.1 \cdot s^{0.8}) \quad (4)$$

where $ktc$ is the transport capacity coefficient (in metres), $s$ is the slope (in $m\ m^{-1}$) and $R$, $K$, $L$ and $S$ are the RUSLE (Renard *et al.*, 1996) factors: $R$ is the rainfall erosivity factor (in $N\ h^{-1}\ a^{-1}$), $K$ the soil erodibility factor (in $kg\ h\ m^{-2}\ N^{-1}$), $L$ the slope length factor (dimensionless), and $S$ the slope gradient factor (dimensionless).

If the sediment inflow plus the local potential erosion calculated by RUSLE at a grid cell exceeds the transport capacity, net deposition occurs. The amount of material leaving this grid cell then equals the transport capacity. The transport capacity coefficient $ktc$ depends on land-use type. It was originally calibrated for a 20 m grid resolution based upon data from 21 catchments in the Belgian Loess Belt, yielding 75 m for non-erodible surfaces (forest and pasture) and 250 m for arable land (Verstraeten *et al.*, 2006). Different grid sizes require a re-calibration of the transport capacity coefficient, whereas Van Oost *et al.* (2003) found an optimum value of about 150 m for cropland for a 5 m grid resolution.

On tilled fields, runoff direction is affected by tillage induced oriented roughness, causing runoff to flow along tillage instead of topographic direction (Desmet and Govers, 1997; Souchère *et al.*, 1998; Takken *et al.*, 1999). To account for a resulting change in runoff and erosion patterns, the logistic regression model developed by Takken *et al.* (2001) was implemented in the calculation of the contributing area as well as that of the water induced sediment and SOC routing. The model includes the slope $s$ (in percentage), the angle between tillage orientation and aspect direction $\alpha$ (in degrees) and the oriented roughness $R_O$ (in centimetres) and is applied to calculate the probability $p$ of runoff flowing in topographic direction:

$$\text{logit}(p) = -5.92 + 0.133 \cdot s + 0.102 \cdot \alpha - 0.417 \cdot R_O \quad (5)$$

The flow direction is predicted to be topographic if the calculated probability is greater than 0·5, and flow is predicted to be in tillage direction if the probability is less than 0·5.

Tillage erosion is caused by variations in tillage translocations over a landscape and always results in a net soil displacement in the down slope direction. The net down slope flux $Q_{til}$ (in $kg\ m^{-1}\ a^{-1}$) due to tillage implementations on a hill slope of infinitesimal length and unit width is calculated with a

diffusion-type equation adopted from Govers *et al.* (1994) and is proportional to the local slope gradient:

$$Q_{til} = k_{til} \cdot s = -k_{til} \cdot \frac{\Delta h}{\Delta x} \quad (6)$$

where $k_{til}$ is the tillage transport coefficient (in kg m$^{-1}$ a$^{-1}$), $s$ is the local slope gradient (in percentage), $h$ is the height at a given point of the hill slope (in metres) and $x$ the distance in horizontal direction (in metres). The local erosion or deposition rate $E_{til}$ (in kg m$^{-2}$ a$^{-1}$) is then calculated as:

$$E_{til} = -\frac{\Delta Q_{til}}{\Delta x} = \frac{\Delta^2 h}{\Delta^2 x} \quad (7)$$

As tillage erosion is controlled by the change of the slope gradient and not by the slope gradient itself, erosion takes place on convexities and soil accumulates in concavities. The intensity of the process is determined by the constant $k_{til}$ that ranges between 500 and 1000 kg m$^{-1}$ a$^{-1}$ in western Europe (Van Oost *et al.*, 2000).

In previous studies (e.g. Poesen *et al.*, 2001; Ruysschaert *et al.*, 2004, 2005), the importance of soil loss due to crop harvesting of root crops has become apparent. According to Auerswald (2006) average losses of soil adhering to sugar beet range from 5 to 8 *t* ha$^{-1}$ a$^{-1}$ in Germany with large annual fluctuations. Since this in the same dimension as soil losses caused by water or tillage erosion and sugar beet provides 33% of the crop rotation in the test site, harvest erosion was also considered for C balancing in this study. It was assumed, that $E_{har}$ is spatially uniform and that the SOC content of the adhering soil equals the SOC content of the plough layer ($SOC_{plough}$). Thus, the amount of SOC removed from the plough layer [$SOC_{loss}$, (in g m$^{-2}$)) is proportional to the ratio between harvest erosion $E_{har}$ (in metres) and the depth of the plough layer $PD$ (in metres):

$$SOC_{loss} = \frac{E_{har}}{PD} \cdot SOC_{plough} \quad (8)$$

Assuming a mean harvest erosion of $\sim 7 \times 10^{-3}$ kg ha$^{-1}$ a$^{-1}$ found for North Rhine-Westphalia (1980–2000) (Auerswald, 2006), $E_{har}$ was set to $5.6 \times 10^{-4}$ m for each sugar beet year in the model.

Soil organic carbon (SOC) dynamics

The ICBM (Andrén and Kätterer, 1997) describes SOC dynamics using two C pools, a so-called young pool, mainly consisting of undecomposed plant residues and roots, and a so-called old SOC pool, comprising the slow and passive pool, and four C fluxes: (1) C input from plants to soil, (2) mineralization from the young and (3) the old pool, and (4) humification, i.e. transformation from the young to the old pool. The dynamics of the two SOC pools are described as:

$$\frac{\Delta Y}{\Delta t} = i - k_Y r Y \quad (9)$$

$$\frac{\Delta O}{\Delta t} = h k_Y r Y - k_O O \quad (10)$$

where $Y$ and $O$ are the young and the old C pool in each soil layer, respectively (in g C m$^{-2}$), and $k_Y$ and $k_O$ are the corresponding turnover rates (in a$^{-1}$). The C input (in g C m$^{-2}$ a$^{-1}$) is $i$, $h$ is the humification coefficient (dimensionless), and $r$ is a climate coefficient (dimensionless), which is assumed to equally effect the decomposition of the young and old pool. The humification coefficient depends on the source of C input and on clay content $cl$ (in percentage):

$$h = \frac{i_c \cdot h_c + i_m \cdot h_m}{i} \cdot e^{0.0112 \cdot (cl - 36.5)} \quad (11)$$

$$i = i_c + i_m, \quad (12)$$

where $i_c$ are inputs of C from crop residues, roots, and rhizodeposition and $i_m$ are inputs from manure (in g C m$^{-2}$ a$^{-1}$), while $h_c$ and $h_m$ are the corresponding humification coefficients. The climate effect accounted for by $r$ primarily depends on mean annual air temperature $T$ (in °C) that is assumed to be spatially uniform. As soil moisture is an important driver of the spatial variability of heterotrophic soil respiration (e.g. Herbst *et al.*, 2009), a spatially variable relative wetness index $WI_r$, calculated from the wetness index $WI$ (Beven and Kirkby, 1979) of each grid cell divided by the arithmetic mean of the $WI$ within the test site, was integrated into the calculation of the climate effect:

$$r = 2.07^{\frac{T-5.4}{10}} \cdot \frac{1}{WI_r} \quad (13)$$

As the $WI_r$ is highest at depositional sites due their large contributing areas and relatively flat slopes, the integration of $WI_r$ accounts for a reduced SOC mineralization under wetter conditions often found in deposits (e.g. Berhe *et al.*, 2007). Since the $Q_{10}$ value of 2.07 (Kätterer *et al.*, 1998) did not differ significantly from the mean $Q_{10}$ value derived from measured soil respiration and soil temperature data in our test site (Fiener *et al.*, 2011), it was not changed from the original model implementation. Also its dependency on temperature, which is based on the mean annual air temperature of 5·4 °C for the test site in Sweden, was adopted. In that study, Andrén and Kätterer (1997) estimated the turnover rates for the plough layer that were set to $k_Y = 0{\cdot}8$ a$^{-1}$ and $k_O = 0{\cdot}006$ a$^{-1}$. The humification coefficients were set to $h_c = 0{\cdot}125$ and $h_m = 0{\cdot}31$, respectively.

The turnover rates of the young and the old pool exponentially decrease with increasing soil depth following Rosenbloom *et al.* (2001):

$$k_{Y/Oz} = k_{Y/Os} \cdot e^{(-u \cdot z)} \quad (14)$$

where $k_{Y/Oz}$ and $k_{Y/Os}$ are the turnover rates (in a$^{-1}$) at depth $z$ (in metres) and at the soil surface, respectively. The exponent $u$ (dimensionless) needs to be calibrated in an inverse modelling approach.

The C input by roots into the soil profile is modelled by an exponential root density function (Van Oost *et al.*, 2005a). Additionally, the C input by plant residues, cover crops and/or organic manure is specified.

SOC redistribution and profile evolution

SOC erosion from the topsoil layer for the young and the old pool ($C_{ero,Y/O}$) is modelled using the results of the water and tillage erosion component as well as those from the soil loss due to crop harvesting routine. It is calculated as

$$C_{ero,Y/O} = SOC_{plough,Y/O} \cdot \frac{M_{ero}}{M_{plough}} \quad (15)$$

with $SOC_{plough,Y/O}$ being the amount of SOC in the plough layer (in grams), $M_{ero}$ being the mass of eroded soil (in grams) and $M_{plough}$ being the total mass of the plough layer (in grams).

At erosion sites, a fraction of SOC from the first subsoil layer proportional to the erosion height is incorporated into the plough layer, since plough depth is maintained during the whole simulation period. Accordingly, SOC from the second subsoil layer is assigned to the first subsoil layer, etc. At depositional sites, the deposition height is used to simulate a change in soil depth. Since plough depth is maintained, a fraction of the SOC proportional to the deposition height is transferred to a buried plough layer that is dynamic and equals the total deposition height. The subsoil layers are also buried in the soil profile.

Since the transport of SOC during water erosion may result in an additional mineralization of SOC and thus in a source of atmospheric C (Lal, 2003), a fixed fraction of the C transported in runoff ($C_{ero,wat}$) (in $g\,C\,m^{-2}\,a^{-1}$) is assumed to be mineralized. Thus, the C loss caused by mineralization of SOC in soil eroded by water ($C_{oxi}$) (in $g\,C\,m^{-2}\,a^{-1}$) can be calculated as

$$C_{oxi} = f_{oxi} \cdot C_{ero,wat} \tag{16}$$

with $f_{oxi}$ (dimensionless) being in the range of zero to one.

## Model implementation

The simulation period was set from 1950, when arable agriculture in the region was intensified due to the introduction of more powerful machinery, to 2007, when SOC inventory measurements were carried out. During this period, a constant crop rotation of sugar beet, winter wheat and winter barley was assumed, although this has been only explicitly documented by the farmer since the 1970s. In 1980, management changed from conventional to conservation agriculture accompanied by the introduction of chisel instead of mouldboard ploughing and a cover crop after sugar beet. The model operates in a yearly time step, and the spatial resolution is 6·25 m × 6·25 m.

### Soil redistribution

The RUSLE (Renard *et al.*, 1996) factors were determined as follows:

i. A *K* factor map (representing soil erodiblity) was derived from a digital soil map (scaled 1:50 000) provided by the Geological Survey of North Rhine-Westphalia, where it was calculated following Deutsches Institut für Normung (2005). The *K* factor ranges from 0·058 to 0·061 $kg\,h\,m^{-2}\,N^{-1}$.
ii. The annual *R* factor (representing rainfall erosivity) and its seasonality were calculated using precipitation data (1975–2007; five minute temporal resolution) from the precipitation station Bockeroth situated about 2·5 km to the east of the test site (151 m a.s.l.) provided by the Landesamt für Natur, Umwelt und Verbraucherschutz Nordrhein-Westfalen (LANUV) following an approach of Schwertmann *et al.* (1987). The annual *R* factor is 88·96 $N\,h^{-1}\,a^{-1}$ with a pronounced seasonality owning highest values in May and June.
iii. The calculation of the *C* factor (representing cropping conditions) for the crop rotation in the test site is also based on Schwertmann *et al.* (1987), whereas regional sowing and harvesting dates were taken from meteorological yearbooks (average of 1995 to 2004) provided by the German Weather Service (DWD). The calculated *C* factor for the modelled period of conventional tillage amounts to 0·142, and for the period of conservation tillage to 0·028, respectively.
iv. The *L* factor (representing slope length) is replaced by the unit contributing area calculated following Desmet and Govers (1996a), and the *S* factor (representing slope) is calculated following McCool *et al.* (1987). Both are simulated throughout the model run based on a digital elevation model (DEM) with a 6·25 m × 6·25 m grid. The DEM was interpolated from LiDAR data (2–3 m point distance) provided by the Landesvermessungsamt North Rhine-Westphalia using ordinary kriging (spherical model; nugget: 0·6; sill: 46·2; range: 237 m) within the Geostatistical Analyst of the Geographical Information System ArcGIS 9.2 (ESRI Inc., USA).
v. Since contour ploughing is carried out in the test site, a *P* factor map (representing soil protection due to specific management) is calculated during the model run accounting for the local slope of each grid cell following Schwertmann *et al.* (1987). The *P* factor in our test site ranges between 0·5 and 0·7.

As no spatially distributed measured soil redistribution data were available for our test site, the transport capacity coefficient (Equation 4) could not be calibrated accordingly. Thus, it was reduced to the optimum value of 150 m derived for a 5 m grid in Van Oost *et al.* (2003). Takken *et al.* (2001) derived characteristic measures of oriented roughness per crop type in a three-year monitoring period of an agricultural catchment in the Belgian Loess Belt. Following this, the oriented roughness (Equation 5) for winter wheat and winter barley was set to 2 cm and that for sugar beet to 3 cm.

The tillage transport coefficient (Equation 6) was set to 600 $kg\,m^{-1}\,a^{-1}$ from 1950 up to 1979 when tillage depth by mouldboard ploughing was 0·25 m, and from 1980 onwards it was set to 400 $kg\,m^{-1}\,a^{-1}$, when tillage depth was reduced to 0·15 m by cultivator tillage assuming 2–3 tillage operations per year. This results in an average of 500 $kg\,m^{-1}\,a^{-1}$ for the whole simulation period corresponding to average tillage erosion intensities over the last 35–45 years derived for various sites across Europe (Van Oost and Govers, 2006).

### Soil organic carbon (SOC)

The C input from plant to soil at the time of harvest is estimated from yield observation in each simulation year. Since yield data were not explicitly available for the test site, data for winter wheat and winter barley were adopted from the agricultural research station Gut Frankenforst (Universität Bonn; approximately 1·5 km southeast of the test site), which have been available since 1965. The data represent mean values of two to 10 fields in each year. Since sugar beet is not cultivated by the research station, corresponding yield data were taken from statistical data of IT NRW (Information und Technik, Nord-Rhein Westfalen) for the administrative unit Rhein-Sieg Kreis, which have been available from 1950 until today. The gap from 1950 to 1965 for winter cereals was filled by regression equations between the Frankenforst and the Rhein-Sieg Kreis data with Pearson correlation coefficients of 0·88 for winter wheat and 0·82 for winter barley, respectively.

The parameterization of the C input from yield data for cereal crops was adopted from Van Oost *et al.* (2005b), where the proportion of C allocated to roots is assumed to constitute 30% of total C assimilation. The grain dry matter yield is assumed to constitute 45% of above ground dry matter, and stubble and other losses of above ground crop residues is set to 15% of above ground biomass. Following this, the root dry matter can be estimated as 95% and the stubble dry matter as 33% of grain dry matter. Carbon input for sugar beet is calculated every third year. Following Draycott (2006), the proportion of fibrous roots and storage roots of total dry matter weight before harvest was set to 3% and 66.5%, respectively. Thus, the dry matter content of fibrous roots corresponds to 4·5% and the

above ground biomass to 45% of the storage root. When specifying mustard as a cover crop before sugar beet, the C input by this cover crop is added to the C input in each sugar beet year. Following Gan *et al.* (2009), mustard roots contribute approximately 23% to total dry matter content, which was set to $4 \times 10^3$ kg per hectare (Aigner, 1998; Frede and Dabbert, 1999). The C content in dry matter for all crops was set to 45%. As the estimation of C input is derived from relationships at harvesting date, it does not consider C released by rhizodeposition (including exudates) (Hütsch *et al.*, 2002) during crop growth. Following Ludwig *et al.* (2007) this input was set to 50% of the C input by crop and root residues for cereals and to 35% of the C input by crop and root residues for sugar beet.

The soil C dynamics model needed to be calibrated in an inverse modelling approach without running the soil redistribution component for the described land management history. Modelled SOC inventories in each soil layer were compared with measured ones at reference sites ($n = 65$) chosen from earlier erosion modelling in the test site (Dlugoß *et al.*, 2010). In several set-up runs, the C input by manure and roots as well as the decline of the turnover rate with depth were iteratively adjusted so that the modelled SOC inventories fit the measured ones. Mean values at reference sites could be well met in the first and second soil layer, whereas a higher deviation, still within the range of ± one standard deviation, was achieved for the deepest soil layer (Figure 2). Adjustments resulted in C input by manure of 10 g C $m^{-2}$ and 60% of roots being in the topsoil layer. The exponent for the reduction of turnover rate with depth $u$ (Equation 14) is set to 2·8, resulting in a mean residence time of ~10 years for the young and ~1360 years for the old pool in the deepest soil layer.

An average, spatially uniform soil bulk density of 1·3 g $cm^{-3}$ in the plough layer and 1·5 g $cm^{-3}$ for the two subsoil layers was implemented. The clay content influencing the humification coefficient was also set as a spatially uniform value of 19% in each soil layer since spatial variability was not very distinct.

For the beginning of the simulation in 1950, a spatially uniform SOC content which is in equilibrium state was assumed for each soil layer, since no data from the initial SOC distribution were available. The results of Van Oost *et al.* (2005a) showed that neglecting the pre-existing erosion history leads to conservative estimations of the erosion induced C fluxes.

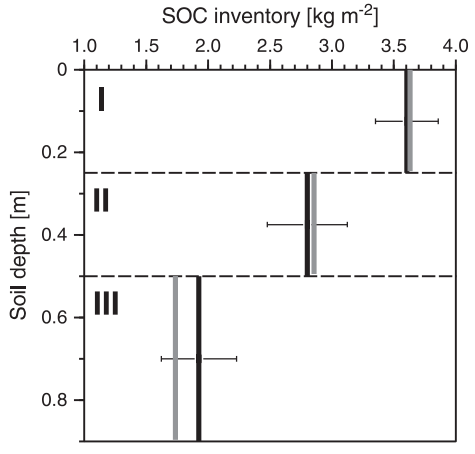


**Figure 2.** SOC inventories at reference sites (sites with erosion or deposition) for three soil layers (I: 0–0·25 m; II: 0·25–0·50 m; III: 0·50–0·90 m). The black line represents the measured arithmetic mean at reference sites ($n = 65$) ± one standard deviation (error bar) for each soil layer. The grey line represents the corresponding modelled value resulting from calibration in an inverse modelling approach.

## Sensitivity analysis

A sensitivity analysis was performed to test the effects of the following uncertainties and assumptions on the mean lateral and vertical C fluxes resulting from soil redistribution processes.

i. To test if the modelled C fluxes are sensitive to the assumption of steady-state spatially uniform SOC contents at the beginning of the simulation, the simulation period was increased to 100 years meaning that pre-existing land management and corresponding erosional processes were considered. A relatively low soil redistribution rate (C factor = 0.02; $k_{til} = 100$) derived from a crop rotation solely consisting of small grains and non-mechanized agriculture and a constant yield were assumed for the period before 1950.
ii. As C inputs to the soil rely on yield data not directly measured at our test site and on relatively simple average relations between yield and C input, we varied the C input by adding and subtracting 50% of the estimated C input in each simulation year without recalibrating the SOC dynamics model.
iii. To account for the fact that modelled soil erosion rates could not be validated against an independent spatially distributed erosion data set, the total soil redistribution rate was changed by varying the tillage transport coefficient and the potential water erosion calculated by RUSLE by ±50% for the two simulation periods. Potential water erosion was changed by changing the USLE *C* factor, since the calculation of this factor is most tentative and since it is related to land management.
iv. As USLE based model approaches assume a constant yearly erosion rate as long as the USLE factors do not change, the model cannot take into account the fact that soil erosion by water is not a continuous process, but is dominated by a few large events, especially at the catchment scale (Edwards and Owens, 1991; Fiener and Auerswald, 2007). In order to explore the importance of temporal variability of water erosion, we performed a simulation where soil erosion by water only occurs every 10 simulation years with a 10-fold magnitude of the average modelled water erosion.

For each sensitivity model run, the C fluxes of the two periods (conventional and conservation tillage) were analysed separately to consider possible effects between different land management and the effect of a change from conventional to conservation agriculture.

# Results and Discussion

## Soil redistribution

The map of modelled cumulative (1950–2007) total erosion (Figure 3), comprising water and tillage induced soil redistribution as well as soil loss due to crop harvesting simulated every third year, shows that the test site can be divided into two parts with regards to the intensity of the erosional processes. The western part of the test site with slopes between 1° and 2° (Figure 1) is dominated by relatively low erosion and deposition rates between −0·05 and 0·05 m in 58 years. In contrast, in the steeper eastern part (slopes up to 9·5°) a spatially distinct pattern of erosion and deposition sites is observed. Highest cumulative total erosion (< −0·2 m) mainly caused by water erosion occurs in the small thalweg area. As no deposition by water is modelled within the test site, the colluvial area

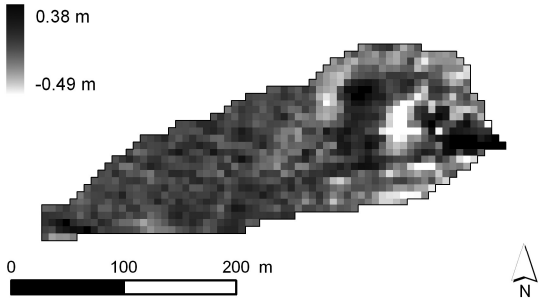


**Figure 3.** Map of modelled cumulative (1950–2007) total erosion; positive values indicate deposition, and negative values indicate erosion.

(deposition > 0·2 m) near the outlet of the test site is formed by tillage induced deposition. Highest erosion by tillage operations is located at the shoulders of the north–south-facing slope in the eastern part of the test site. This corresponds to other results in the literature (e.g. Govers *et al.*, 1994), where tillage induced erosion generally occurs on convexities and on the down slope sides of field boundaries, whereas deposition caused by tillage processes occurs on concavities and on the upslope sides of field boundaries.

The modelled cumulative deposition rates in the colluvial area near the outlet of the test site are in qualitative agreement with measured radiocarbon and corresponding SOC and texture data (Figure 4). In general, the chosen soil profiles at the reference sites (modelled cumulative soil redistribution rates of $-0{\cdot}01$ m 58 $a^{-1}$ for both points), the erosion sites [modelled cumulative soil redistribution rate of $-0{\cdot}22$ m 58 $a^{-1}$ (E1) and $-0{\cdot}21$ m 58 $a^{-1}$ (E2)] and the deposition sites (modelled cumulative soil redistribution rate of 0·38 m 58 $a^{-1}$ (D1) and 0·12 m 58 $a^{-1}$ (D2)] show a typical behaviour for water erosion with respect to sand and for total erosion with respect to SOC content. In comparison with the reference and the erosion profiles, the depositional profiles are generally enriched in sand, which is indicative of a preferential deposition of coarse material. This is counterintuitive to the model results as no deposition by water is modelled at the two profiles. This may indicate three processes that are not taken into account in the model: (i) deposition of coarse material during net erosion, (ii) a backwater effect resulting from runoff entering the downslope grass strip (especially at D1), and/or (iii) deposition during large transport limited events that are not accounted for in the yearly time step of the model. With respect to SOC content no substantial differences were found in the topsoil layers at all profiles. However, the decrease of SOC with depth is most pronounced at the erosion profiles and less steep at the reference profiles. At the depositional site, an accumulation of SOC throughout the whole soil profile can be observed.

A similar relation between the three profiles could also be found with respect to the AMS radiocarbon data (Figure 4). In the plough layer, $^{14}C$ contents did not show any substantial differences between the six profiles with values ranging between 98 and $100 \pm 0{\cdot}4$ pMC. But in contrast to results from Rethemeyer *et al.* (2005) on undisturbed maize and wheat fields in Germany, the values are below the actual atmospheric $^{14}C$ concentration at the date of sampling (104·7 pMC in 2009). This indicates that besides young C from recent plant residues, substantial amounts of older SOC pools exist in the plough layer at our test site. In addition, relative differences between the $^{14}C$ depth profiles of the different landscape positions can be observed. The erosion and reference profiles show a decrease of $^{14}C$ with depth presumably caused by a higher relative abundance of old SOC pools with increasing soil depth being most pronounced at the erosion site. In contrast, at the depositional site, $^{14}C$ contents remain as high as in the topsoil layer or slightly increase to values higher than $100 \pm 0{\cdot}4$ pMC up to 0·6 m in depth at D1 and up to 0·4 m in depth at D2. This indicates the abundance of younger SOC as compared to same depth increments at the erosion and reference sites. Below this depth, $^{14}C$ values decrease to values similar to the reference and erosion sites. Since $^{14}C$ contents in excess of 100 pMC must be attributed to the so-called bomb curve, the high $^{14}C$ contents at depth must have been imprinted since the 1950s. These high radiocarbon concentrations were not found below the plough layer at the reference and the erosion site. Thus, the high $^{14}C$ values found at D1 and D2 can only be attributed to depositional processes. Simply estimating deposition from the depth interval with increased $^{14}C$ contents below the plough layer revealed that deposition had not exceeded 0·45 m at D1 (deposition rate: 7·5 mm $a^{-1}$) and 0·3 m at D2 (deposition rate: 5 mm $a^{-1}$) since 1950. The reconstruction of the depth interval with increased $^{14}C$ concentrations at the depositional profiles resulted in similar estimates (Figure 5). The measured $^{14}C$ depth distributions were best reproduced using a deposition rate of 7 mm $a^{-1}$ and 5 mm $a^{-1}$ at D1 and D2, respectively, in the modified bomb $^{14}C$ model of Harkness *et al.* (1986) (Equations 1–3). The application of different

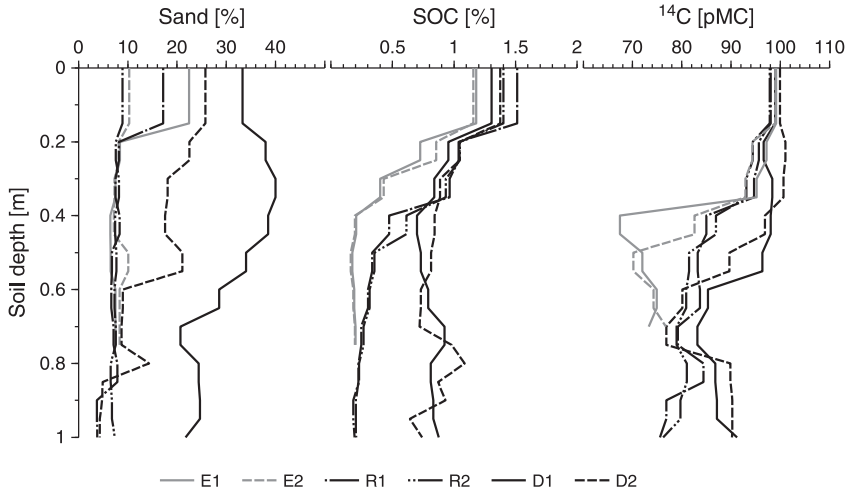


**Figure 4.** Depth distribution of sand, SOC and $^{14}C$ content of bulk soil samples at different slope positions. R, D, and E represent reference, deposition, and erosion sites, respectively.

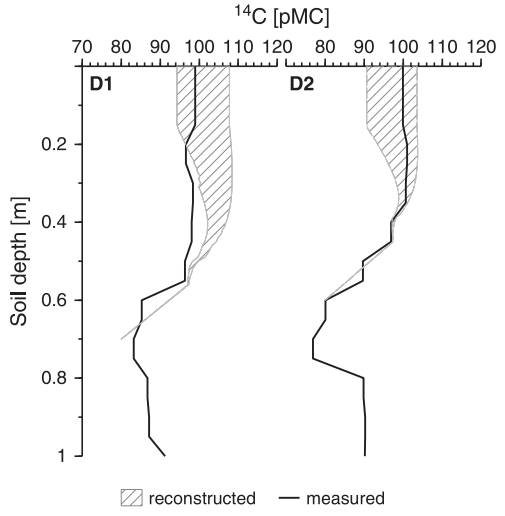


**Figure 5.** Depth profiles of the measured and reconstructed $^{14}C$ content at the two depositional sites. For the reconstructed depth distributions different erosion rates were applied.

erosion rates (Figure 5) showed, that the depth interval of increased $^{14}C$ contents did not depend on the origin of the deposited soil and hence its depletion in $^{14}C$, but just on the deposition rate so that the method can be used to derive deposition rates since the 1950s without further knowledge of the origin of the deposited soil. Comparing these values with the modelled deposition rates (6·5 and 2·3 mm $a^{-1}$ at D1 and D2, respectively) reveals that SPEROS-C slightly underestimated deposition at both profiles. This might again be an indication for additional deposition during water erosion processes which is not modelled.

Due to the change from conventional to conservation agriculture in 1980, a distinct reduction of water and tillage erosion was modelled in the second simulation period. Mean net water erosion dropped from 0·66 to 0·13 mm $a^{-1}$ for 1950–1979 and 1980–2007, while the net tillage erosion reduced from 0·79 to 0·55 mm $a^{-1}$ (Table I). Whereas the individual spatial patterns of both erosion processes remained stable for the two simulation periods, the spatial pattern of total erosion combining both processes changed leading to an increase of the depositional area from 26% to 39% within the test site (Table I).

Similar to the two test sites in Van Oost *et al.* (2005b), erosion by tillage is the dominant process, accounting for ~71% in the phase of conventional tillage and ~91% in the phase of conservation tillage, respectively.

## Soil organic carbon (SOC) stocks

In general, the measured SOC inventory patterns in each soil layer (Figure 6A) are linked to modelled soil redistribution patterns with low SOC values at the erosional sites and high SOC contents at the depositional sites as was already shown in an earlier study within the test site (Dlugoß *et al.*, 2010). This pattern is more pronounced in deep soil layers and leads to a higher spatial variability of measured SOC in the two subsoil layers as compared to the plough layer. This result is confirmed by the coefficients of variation of SOC which equal 8% in the plough layer and 20% and 44% in the two subsoil layers, respectively.

Another area of relatively high measured SOC contents, primarily in the two upper soil layers is located in the upper part near the southern boundary of the test site (Figure 6A). At this relatively flat slope position, these high values cannot be attributed to soil redistribution processes, but we assume that they were caused by former dung or sugar beet storage.

**Table I.** Statistics of modelled water ($E_{wat}$), tillage ($E_{til}$) and total erosion ($E_{tot}$) within the test site ($n = 1030$) for the modelled period of conventional (1950–1979) and conservation tillage (1980–2007), as well as for the whole simulation period (1950–2007) differentiated into erosional (E) and depositional (D) sites.

| | | Soil erosion (mm $a^{-1}$) | | | | | |
|---|---|---|---|---|---|---|---|
| | | $E_{wat}$ | | $E_{til}$ | | $E_{tot}$ | |
| | | E | D | E | D | E | D |
| 1950–1979 | Mean | 0·66 | — | 0·79 | 1·11 | 1·11 | 0·68 |
| | SD | 1·37 | — | 0·65 | 1·55 | 1·23 | 0·96 |
| | Max | 16·88 | — | 3·17 | 10·25 | 14·32 | 7·30 |
| | *n* | 1030 | 0 | 588 | 442 | 761 | 269 |
| 1980–2007 | Mean | 0·13 | — | 0·52 | 0·74 | 0·57 | 0·62 |
| | SD | 0·27 | — | 0·43 | 1·03 | 0·47 | 0·86 |
| | Max | 3·33 | — | 2·11 | 6·83 | 2·38 | 6·25 |
| | *n* | 1030 | 0 | 588 | 442 | 632 | 398 |
| 1950–2007 | Mean | 0·41 | — | 0·66 | 0·93 | 0·85 | 0·61 |
| | SD | 0·84 | — | 0·54 | 0·96 | 0·82 | 0·87 |
| | Max | 10·33 | — | 2·66 | 7·30 | 8·18 | 6·79 |
| | *n* | 1030 | 0 | 588 | 442 | 700 | 330 |

Note: SD, standard deviation; Max, maximum; *n*, number of grid cells in the test site.

The modelled SOC inventory patterns of the three soil layers (Figure 6B) are generally in good agreement with the measured patterns. Lowest values can be found along the thalweg (water erosion) and on the shoulders of the north–south-facing slope (tillage erosion), whereas highest SOC contents in each soil layer are located in the modelled depositional area near the outlet of the test site. The other area of relatively high observed SOC contents in soil layers I and II, is potentially related to processes not included in the model and could therefore not be reproduced by SPEROS-C, resulting in moderate modelled SOC contents in this area.

To more explicitly analyse which areas can be well described by SPEROS-C and which ones show potential gaps in process description, we divided the measured and modelled SOC stocks into classes of cumulative (1950–2007) total erosion (Figure 7). These comprise two classes of moderate to high erosion ($< -0{\cdot}1$ m), two classes of moderate to high deposition ($> 0{\cdot}1$ m), and three classes of low erosion or deposition (between $-0{\cdot}05$ and $0{\cdot}05$ m).

In the plough layer, modelled mean SOC inventories lie close to the 1:1 line (Figure 7) except for the maximum erosion ($< -0{\cdot}2$ m) class, where depletion of SOC is slightly overestimated. On the one hand, this might indicate a slight overestimation of erosion or an underestimation of dynamic replacement at sites of extreme erosion. On the other hand, this maximum erosion class is dominated by five grid cells located along the thalweg of the catchment. In case of a raster based model, the high erosion rates resulting from concentrated erosion along the thalweg are attributed to the total area of this grid cell, while point measurements of SOC within the grid cell might or might not represent a linear feature smaller than the overall grid cell. Hence, we assume that the mismatch between measured and modelled SOC inventory in this erosion class potentially results from the relatively small number of grid cells and from differences representing space in SPEROS-C compared to the measured inventory.

In the first subsoil layer, SOC in the maximum erosion class is also slightly underestimated, whereas SOC in the maximum deposition class is overestimated by SPEROS-C. This is in contrast to the results of Van Oost *et al.* (2005a), who found an underestimation of SOC accumulation in this soil depth. However, as the maximum class just comprises ~1% of the

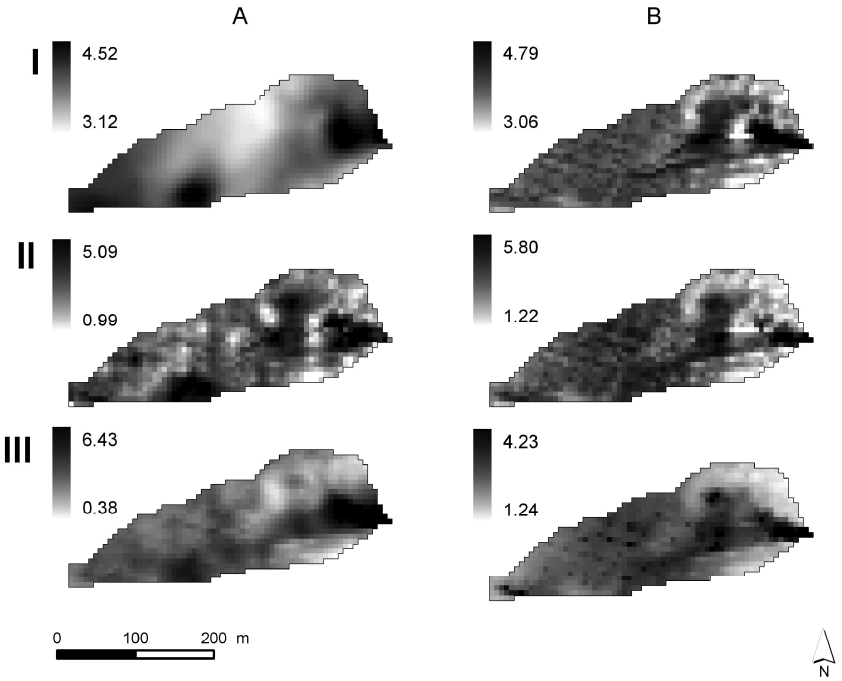


**Figure 6.** Maps of measured (A) and modelled (B) SOC inventories (in kg $m^{-2}$) for the three soil layers (I: 0–0·25 m; II: 0·25–0·50 m; III: 0·50–0·90 m).

total catchment area and the mean values of all other classes lie close to the 1:1-line, SPEROS-C reproduces the spatial variability of SOC contents in the first and second soil layers very well.

In the deepest soil layer especially high measured SOC values of the high deposition classes are underestimated by the model (Figure 7). On the one hand, this underestimation might be attributed to a general slight underestimation resulting from inverse estimation of the SOC model parameters at reference sites in this soil layer (Figure 2). This is also visible in Figure 7, where the mean of the class without erosion or deposition is situated slightly below the 1:1 line for the deepest soil layer, whereas this class is perfectly represented in the two upper layers. On the other hand, the underestimation of C storage by deposition in that soil layer might be caused by the fact that our simulation started in 1950 with a spatially uniform start value. Pre-existing soil redistribution history was thus not considered, which might date back to AD ~1500 when agricultural use began in the region (Preston, 2001). Our detailed profile data from two depositional sites (Figure 4) indicate historic deposition below 0·5 m depth, as they show a substantial enrichment in sand, SOC and AMS $^{14}$C, when compared to the reference and erosional profiles. Trying to reconstruct the measured $^{14}$C depth distribution at the two depositional profiles using the modelled deposition rates at these points (Figure 5) also indicates an underestimation of deposition especially at D2. In their experimental study Van Hemelryck *et al.* (2010) hypothesized that turnover of SOC might be lower at depositional compared to erosional sites, especially in the deeper soil layers because of the production of a dense sediment layer capping the soil surface and thus hampering gas exchange. Hence, turnover of SOC might also be overestimated in this subsoil layer. In concordance to the modelled results of the two upper soil layers, the mean SOC inventory of the maximum erosion class is underestimated in the deepest soil layer compared with the measured data. Again this can be deduced by the fact that this class is dominated by five grid cells lying in a line of concentrated flow.

The overall spatial variability of SOC as expressed in the range of data (Figure 6) is simulated well in the two upper soil layers, whereas it is significantly poorer in the deepest soil layer with a modelled coefficient of variation of ~15%. The same is true for the variability within one soil erosion class (Figure 7), indicating that further spatially differentiating processes need to be considered, especially within the deepest soil layer.

However, values describing the goodness-of-fit between measured and modelled SOC inventories (Table II) display a better overall representation of the modelled results in the two subsoil layers as compared to the plough layer, indicating a close relationship between spatial patterns of soil redistribution and of SOC pools in the deeper soil layers, supporting previous results by Dlugoß *et al.* (2010). In layer II, 28% and in layer III 41% of the SOC variance can be ascribed to the variance of simulated soil redistribution processes. In the plough layer, this relationship is less pronounced due to homogenization by tillage operations, the relatively high turnover rates in that soil layer, and the site-specific high SOC contents in the southern part of the test site resulting from former dung or sugar beet deposits. The specification of the modelled spatial variability is dominated by the redistribution of the old SOC pool, whereas high turnover rates lead to a relatively low spatial variability of the young pool in each soil layer. This is due to the fact that the young pool only comprises about 10% of the total organic C pool throughout the soil profile. In contrast, the mean error and the root mean square error increase with increasing soil depth (Table II), indicating that the modelled SOC inventories are more biased in the deepest soil layer. In general, the overall representation of the measured SOC inventories by the application of SPEROS-C is good, indicating a good process representation concerning the interaction of soil redistribution and soil C dynamics in the model. However, the goodness-of-fit is significantly degraded by a few grid cells that undergo extreme erosion and deposition as well as by the fact, that the area of high SOC contents caused by dung or sugar beet storage was not related to processes integrated in the model.

## Lateral and vertical C fluxes

To determine the long-term (1950–2007) development of net vertical C fluxes between soil and atmosphere resulting from land management and generally increasing yields and to

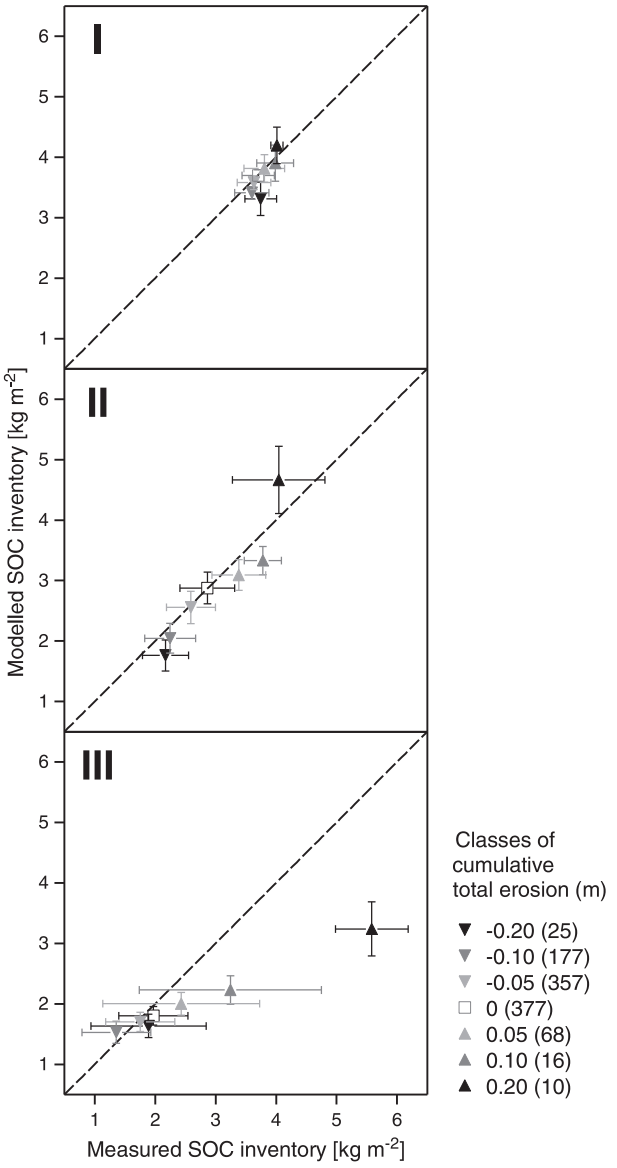


**Figure 7.** Scatter plots of modelled versus measured SOC inventories for three soil layers (I: 0–0·25 m; II: 0·25–0·50 m; III: 0·50–0·90 m). Data are summarized to classes of cumulative (1950–2007) total erosion. The number of grid cells within each class is given in brackets. Data points represent arithmetic means for each erosion class ± one standard deviation. The dashed line represents the 1:1 line.

**Table II.** Values describing the goodness-of-fit [ME, mean error; RMSE, root mean square error; MEF, model efficiency (Nash and Sutcliffe, 1970); *R*, Pearson correlation coefficient] between measured and modelled SOC inventories for the three soil layers (I: 0–0·25 m; II: 0·25–0·50 m; III: 0·50–0·90 m) ($n = 1030$).

| | Soil layer | | |
|---|---|---|---|
| | I | II | III |
| ME | 0·06 | 0·07 | 0·12 |
| RMSE | 0·31 | 0·51 | 0·70 |
| MEF | −0·13 | 0·15 | 0·28 |
| *R* | 0·27 | 0·53 | 0·64 |

separate these C fluxes from those induced by soil redistribution, a first model run was performed without taking erosion into account. In general, the cultivation of sugar beet (starting in 1953, then every third year) lead to a depletion of SOC in the test site, whereas the following cultivation of winter cereals again increased SOC contents (Figure 8). Since yields did not significantly increase between 1950 and 1970, the applied crop rotation acted as a source of atmospheric $CO_2$ under conventional farming in those years. In the following decade, a rapid increase in yields generated a C sequestration in the formerly depleted soils. Thus, the entire period of conventional agriculture was modelled as a small sink of atmospheric C (mean vertical C flux 1950–1979: 1·8 g C $m^{-2}$ $a^{-1}$).

From 1980 to 2007 (period of conservation agriculture), the system became a stronger C sink caused by further increasing yields on the one hand and by the incorporation of mustard as a cover crop on the other hand (mean vertical C flux 1980–2007: 25·2 g C $m^{-2}$ $a^{-1}$). The biomass and its allocated C of the cover crop are completely incorporated into the soil in each sugar beet year before sowing of the winter cereals. Aboveground biomass of mustard contributes to two thirds of the total biomass and is completely incorporated in the plough layer so that the sink term is mainly caused by an increase of SOC in the plough layer. Single sugar beet years still act as a C source to the atmosphere in the period of conservation tillage, but this source term is less pronounced than in the period before. The increasing sink term due to increasing yields might be somewhat overestimated since the relation between yields and C input into the soil remains constant throughout our simulated period. This may not be realistic because an increase in yield due to the cultivation of new crop species does not necessarily result from higher photosynthesis but from allocating more C to harvestable plant parts, thus reducing the C input into the soil (Janzen, 2006; Billings *et al.*, 2010). However, there were no data available that took this aspect into account.

Compared with the catchment integrated mean vertical C flux caused by the applied land management for the whole simulation period (1950–2007: 13·1 g C $m^{-2}$ $a^{-1}$), the catchment integrated mean vertical C flux induced by soil redistribution processes for the whole simulation period represents only ~6% of the total vertical C flux (1950–2007: 0·8 g C $m^{-2}$ $a^{-1}$) (Figure 9). For the period of conventional tillage, the soil redistribution associated vertical C flux contributes to 27% of the total vertical C flux being reduced to approximately 4% in the period of conservation tillage. This corresponds to results of Yadav and Malanson (2009) who found that the vertical C flux associated with erosion or deposition varies with the type of management practice. In cases with conservation

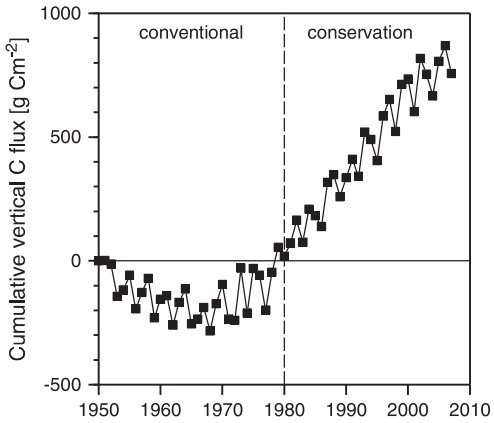


**Figure 8.** Temporal evolution of test site integrated cumulative vertical C flux without simulating soil redistribution; negative fluxes represent a loss, and positive fluxes represent a gain. The modelled time span encompasses a period of conventional (1950–1979) and a period of conservation (1980–2007) agriculture.

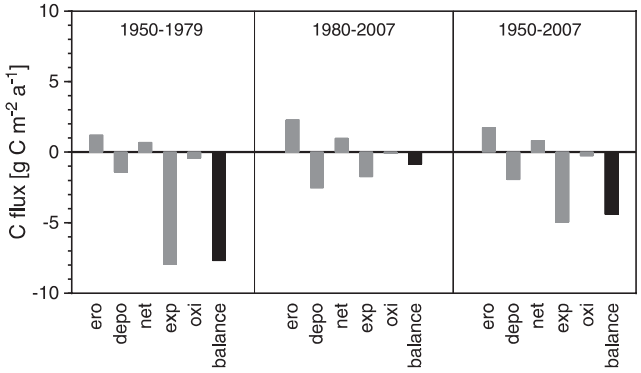


**Figure 9.** Test site integrated mean lateral and vertical C fluxes induced by soil redistribution processes for the modelled period of conventional (1950–1979) and conservation tillage (1980–2007) as well as for the whole simulation period (1950–2007). Negative fluxes represent a loss, and positive fluxes represent a gain (ero: mean vertical C flux at erosional sites; depo: mean vertical C flux at depositional sites; net: mean vertical C flux for the whole catchment; exp: C exported by water erosion; oxi: oxidized C during transport; balance: sum of mean vertical C flux, oxidized and exported C).

practices, the soil redistribution induced C flux was less than 10% of the total C flux, whereas it contributed to almost 50% for non-conservation practices in their test site (Yadav and Malanson, 2009).

Despite its relatively low mean contribution to the catchment averaged vertical C flux, in concordance to the results of Van Oost *et al.* (2005a), the vertical C flux induced by soil redistribution exhibits a very distinct spatial pattern of sink and source areas (Figure 10). Areas with highest deposition constitute the largest sources to the atmosphere (maximum C efflux of ~15 g C $m^{-2}$ $a^{-1}$) mainly by the enhanced mineralization of buried C below the plough layer, whereas areas with high erosion rates act as C sinks due to dynamic replacement (maximum C sequestration of ~15 g C $m^{-2}$ $a^{-1}$).

Thus, in general, the catchment averaged vertical C flux is highly dependent on the relation of erosional and depositional sites. Considering the entire simulation period, on average total erosion occurs on almost two thirds of the test site area with a mean vertical C flux into the soil of 1·7 g C $m^{-2}$ $a^{-1}$, whereas the depositional areas have a mean vertical C flux from soil to atmosphere of 1·9 g C $m^{-2}$ $a^{-1}$ (Figure 9). Thus, the net soil redistribution induced vertical C flux within the whole catchment acts as a small C sink. Only a small amount of modelled C (0·3 g C $m^{-2}$ $a^{-1}$) is oxidized during transport by water. Integrating this C source to the atmosphere and the loss of C due to the export by water erosion (Figure 9), the overall mean C balance (1950–2007) of our test site becomes negative (−4·4 g C $m^{-2}$ $a^{-1}$). This is mainly caused by the fact

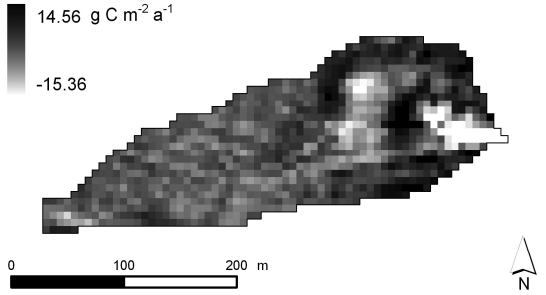


**Figure 10.** Spatial distribution of mean (1950–2007) vertical C flux caused by soil redistribution. Negative fluxes represent a loss, and positive fluxes represent a gain.

that erosion by water is not transport limited in our test site, so that all eroded sediment and C is exported out of the test site.

The reduction of the amount of exported C from ~8 g C $m^{-2}$ $a^{-1}$ during conventional tillage to less than 2 g C $m^{-2}$ $a^{-1}$ during conservation tillage indicates that it is strongly affected by land management practices. Mainly this reduction of water exported C leads to a less pronounced negative C balance (−0·85 g C $m^{-2}$ $a^{-1}$) under conservation agriculture, as compared to conventional practices. In addition, the mean C balance under conservation tillage is reduced due to the fact that the vertical C flux induced by soil redistribution is more positive in the period of conservation tillage compared to that of conventional tillage (Figure 9). This is caused by higher negative fluxes at depositional sites and higher positive fluxes at erosional sites. On the one hand, this is a consequence of the transient nature of the vertical C fluxes (Van Oost *et al.*, 2009) and on the other hand of land management change. The erosion induced C fluxes in the period of conservation tillage are dominated by vertical C fluxes, whereas the period of conventional tillage is dominated by a C loss due to the export by water.

Our results correspond to the findings of Izaurralde *et al.* (2007). Soil respiration contributed to 96% of the erosion induced C loss at their two test sites under no-till treatment. These two test sites were C sinks, whereas the test site under conventional tillage acted as a C source. Even more differentiated results were derived by Billings *et al.* (2010) who found that soil management practices that maintain low erosion rates and high C inputs result in a minimal erosion induced C exchange with the atmosphere at sites with low SOC content or a small net C sink at sites with higher SOC contents. In contrast, management practices promoting high erosion rates and low C input into the soil represent a strong erosion induced C source at sites with low SOC contents, whereas at sites with higher SOC contents, soil redistribution might act as a C source or sink.

In general, the C sink or source term of soil redistribution strongly depends on the fate of the exported C by water erosion (e.g. Berhe *et al.*, 2007; Van Oost *et al.*, 2007). Following Stallard (1998), two thirds of the eroded sediment are stored in the same catchment, in local wetlands or other depositional sites. In the test sites analysed in Van Oost *et al.* (2007), up to 95% of the eroded C was redeposited within the catchments. Since a grass buffer strip of *c.* 50 m width adjoins our test site near the outlet, we assume that most of the sediment and associated C exported by water is trapped there (e.g. Fiener and Auerswald, 2003). Additionally, evidence of water induced deposition near the outlet is given by a change in soil texture owing to an increased sand content of up to 35–40%, as compared to a mean sand content of ~12% for the whole catchment.

Our measured flume data for the Dissenbach catchment (~150 ha), wherein the Heiderhof test site is located, exhibit a mean annual sediment yield of 205 g $m^{-2}$ $a^{-1}$ (2007–2009), which is in the same magnitude as the amount of modelled exported sediment from the Heiderhof test site for the period of conservation tillage (mean 1980–2007: ~170 g $m^{-2}$ $a^{-1}$). This similar sediment yield on the different spatial scales is somewhat surprising, especially as there are grass buffer strips along most of the Dissenbach, but probably results from the fact that most fields in the catchment are still conventionally managed. The mean C content of the exported sediment at the San Dimas flume is ~4%, which constitutes an enrichment factor of 2·7, as compared to a mean SOC content in the plough layer of ~1·5% within the Dissenbach catchment (data derived from a digital soil map (1:50 000) of North-Rhine Westphalia; Geological Survey). This results in a mean C export of 8 g $m^{-2}$ $a^{-1}$ for the

whole Dissenbach catchment in the period 2007 to 2009. The fact that the water exported sediment is enriched with SOC was not accounted for in our model run. Thus, C loss by water export of the Heiderhof catchment is potentially underestimated even under conservation tillage.

## Sensitivity of erosion induced lateral and vertical C fluxes

Non-uniform SOC contents at the beginning of the investigated time period (1950), introduced by a prolonged simulation period (1850–2007), did not substantially change the mean C balance in the considered period of conventional (1950–1979: –7·41 g C $m^{-2}$ $a^{-1}$) and conservation agriculture (1980–2007: –0·53 g C $m^{-2}$ $a^{-1}$). This is caused by the fact, that the C balance in our test site is dominated by the C export by water. Considering vertical C fluxes, the C sink strength of erosion sites (mean vertical C flux 1950–2007: 2·21 g C $m^{-2}$ $a^{-1}$) and the C source strength of deposition sites (mean vertical C flux 1950–2007: –2·28 g C $m^{-2}$ $a^{-1}$) increases with a prolonged simulation period due to the transient nature of these fluxes. However, the extent of this effect is highly dependent on the land management assumptions that affect C inputs as well as soil redistribution for the period before 1950. Assuming extensive grain crop rotations and thereby relatively small erosion rates and C inputs did not change the results for the test site substantially. Hence, it seemed to be reasonable to start the simulation in 1950 and to ignore long-term erosion due to historic land management of which no profound data are available.

In contrast, the lateral and vertical C fluxes associated with soil redistribution exhibit a more pronounced sensitivity to changes of C inputs from plant to soil (Figure 11A). The sink term of the erosion sites as well as the source term at the depositional sites increases with higher C inputs, whereas they are smaller with lower C inputs. This corresponds to results by Billings *et al.* (2010) who found that increasing the SOC production increases the potential C sink at eroding sites as a result of enhanced dynamic replacement. Since the proportion of erosional to depositional sites remains constant, the catchment averaged net vertical C flux increases with increasing C input. However, the overall changes of the vertical C fluxes due to changes in C input are relatively low, whereas the change in the amount of water-exported C, especially under conventional agriculture, is more pronounced. This indicates that under constant soil erosion an increase in soil C inputs increases the C loss of our test site.

The change of the C fluxes caused by the change of total erosion shows a more distinct picture (Figure 11B). The overall C balance of our test site exhibits a linear development in relation to changes in total erosion, i.e. an increase of the source term with increasing total erosion. Increasing the potential total erosion by more than 30%, results in a transport limitation under conventional tillage in our test site, which lead to deposition by water and thus a reduction of the C export. Due to the overall smaller erosion such behaviour was not found under conservation tillage. In each of the two land management periods, the sink function of erosional sites becomes stronger with increased erosion rates. This indicates that the absolute dynamic replacement rate increases with increasing soil erosion as long as yields do not decline. At depositional sites the source term decreases with enhanced soil erosion rates. This results from the deposition of C depleted soil originating from the erosional sites where subsoil material is also eroded with enhanced erosion rates. In general, changes of total erosion again have a higher impact on the lateral than on the vertical C fluxes

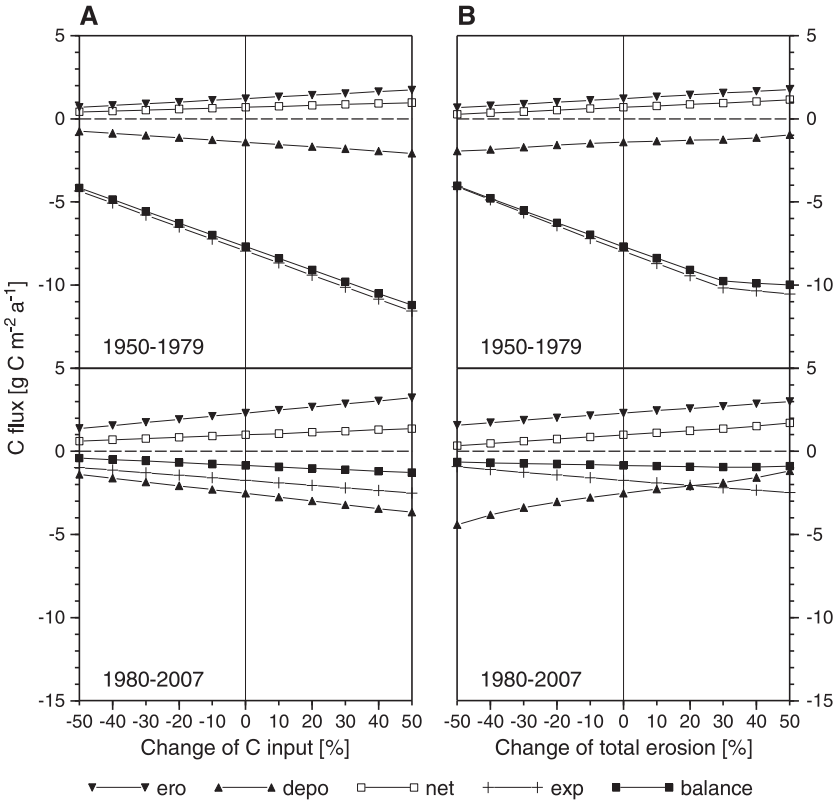


**Figure 11.** Sensitivity of test site integrated mean lateral and vertical C fluxes (in g C $m^{-2}$ $a^{-1}$) induced by soil redistribution processes to changes of C input (in percentage) (A) and changes of potential total erosion (in percentage) (B) for the modelled period of conventional (1950–1979) and conservation tillage (1980–2007). Negative fluxes represent a loss, and positive fluxes represent a gain. Zero change in C input and total erosion corresponds to the results of the reference run (ero: mean vertical C flux at erosional sites; depo: mean vertical C flux at depositional sites; net: mean vertical C flux for the whole catchment; exp: C exported by water erosion; balance: sum of mean vertical C flux, oxidized and exported C).

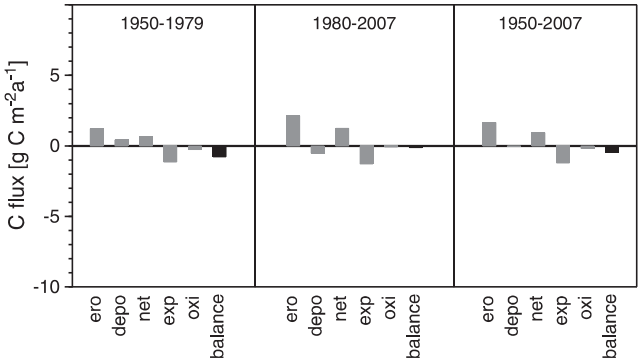


**Figure 12.** Test site integrated mean lateral and vertical C fluxes induced by soil redistribution processes for the modelled period of conventional (1950–1979) and conservation (1980–2007) tillage as well as for the whole simulation period (1950–2007) when water erosion is restricted to every tenth simulation year with a 10-fold average annual water erosion. Negative fluxes represent a loss, and positive fluxes represent a gain (ero: mean vertical C flux at erosional sites; depo: mean vertical C flux at depositional sites; net: mean vertical C flux for the whole catchment; exp: C exported by water erosion; oxi: oxidized C during transport; balance: sum of mean vertical C flux, oxidized and exported C).

especially in the first model period. Especially a change in water erosion processes, i.e. the introduction of deposition by water, clearly shifts the linear behaviour of the C balance. As under conservation agriculture the overall C balance is dominated by the vertical C fluxes, its sensitivity to changes in erosion rates is less pronounced.

The restriction of water erosion to every tenth simulation year (with 10-fold long-term mean erosion) has a strong effect on the lateral and vertical C fluxes in both simulation periods. In contrast to the reference run (model run without any changes of C input or erosion) under conventional tillage, the depositional sites are characterized by a positive vertical C flux to the soil. In the period of conservation tillage, the source strength at depositional sites is significantly reduced compared to the reference run (Figure 12). This can be explained by the fact that in years when water erosion occurs, the depositional sites exhibit a strong sink term, whereas in years when just tillage erosion occurs they act as a C source to the atmosphere. As was the case in the runs with increased total erosion, restricting water erosion to a few large events, leads to a lateral transfer of C depleted subsoil material that is redeposited at the depositional sites and thus reduces mineralization. Since the mean modelled C export by water erosion is significantly reduced especially under conventional tillage ($-1{\cdot}15\,g\,C\,m^{-2}\,a^{-1}$) due to transport limited conditions in case of extreme erosion events, and since the mean vertical C flux at depositional sites is almost zero considering the whole simulation period, the overall effect of soil redistribution on C fluxes at our test site is reduced by almost 90%. Even if we deal with a rough estimate here, e.g. as the used model cannot simulate gully erosion and sediment transport under concentrated flow conditions, the results are a first hint that many studies (e.g. Stallard, 1998) (globally) estimating the effect of soil redistribution on C balances and being based on long-term average erosion rates, may be misleading. Moreover, it also indicates that the mean C exported by water erosion might be overestimated in our reference run.

## Conclusions

At our test site, measured spatial patterns of SOC stocks in three soil layers (0–0·9 m) were closely linked to soil redistribution patterns. In general, SOC depletion was determined at erosional sites and SOC accumulation was determined at depositional sites. Thus, the application of SPEROS-C, which dynamically couples a spatially distributed soil erosion model (including tillage and water erosion) and a SOC model, allowed for the analysis of the spatial patterns of SOC stocks as well as their lateral and vertical fluxes in our test site. The model was applied from 1950 to 2007 in a one-year time step, comprising a period of conventional tillage (1950–1979) followed by a period of conservation tillage (1980–2007) with reduced soil erosion rates and an additional C input by the cultivation of a cover crop.

In general, modelled SOC patterns corresponded well with the measured ones in each soil layer, although there were some discrepancies on areas with extreme erosion or deposition rates. However, these areas only represent ~3% of the total test site area. Two measured AMS $^{14}C$ depth profiles in the colluvial area indicate that modelled deposition is slightly underestimated, possibly caused by the fact that no deposition by water is modelled near the outlet of the test site.

The lateral and vertical C fluxes induced by soil redistribution show a strong relation to land management practices. Whereas the period of conventional tillage is dominated by lateral C fluxes leading to an overall C loss of $7{\cdot}7\,g\,C\,m^{-2}\,a^{-1}$, the period of conservation tillage is dominated by vertical C fluxes reducing the C balance to a loss of $0{\cdot}9\,g\,C\,m^{-2}\,a^{-1}$.

Although it can be expected that the main part of the water exported C from the Heiderhof test site is deposited in an adjacent grass buffer strip, its modelled sediment yield is similar to the sediment yield from the overall Dissenbach catchment which is mostly under conventional agriculture. As the C exported from the Dissenbach catchment exhibits a SOC enrichment factor of 2·7 it can be assumed that our modelled C loss for the Heiderhof test site that does not account for any enrichment is a conservative estimate.

Analysing the sensitivity of C sources and sinks to changes in C input reveals that all C fluxes associated with soil redistribution are enhanced with increasing C input and attenuated with decreasing C input. This indicates that an increase in C input solely does not increase SOC pools when soil erosion rates remain constant, but that for the sequestration of C in soils, soil erosion has to be reduced correspondingly.

Changes in total erosion also exhibit a strong effect on the soil redistribution induced C fluxes. Especially when restricting the occurrence of water erosion to every tenth simulation year with 10-fold increase of erosion, lateral C loss by water as well as atmospheric C source at depositional sites are significantly reduced. This indicates that estimates of the erosion induced sink or source strength might be overestimated when mean annual soil erosion rates are used.

All model runs show a substantial carry over effect of the period of conventional to the following period of conservation agriculture concerning the C fluxes, which is caused by the applied crop rotation as well as those caused by soil redistribution. The applied crop rotation leads to a depletion of SOC in our field in the first model phase, whereas this depletion is compensated in the following phase due to increasing yields and conservation practices. The erosion induced vertical C fluxes are pronounced, whereas the lateral C fluxes are reduced under conservation agriculture (encompassing a reduction of soil redistribution and an increase in soil C input), both leading to a stronger erosion induced atmospheric C sink and a lower lateral C loss.

In general, the spatially distributed SOC and soil redistribution model SPEROS-C proved to be reasonably applicable at the small scale Heiderhof catchment. The adaptations of the model carried out in this study allow for the integration of

different land management, which is important with respect to erosion induced lateral and vertical SOC fluxes. Thus, the model will be applicable to larger spatial scales with spatial variances of land management as well as complex management histories, expanding the possibilities to analyse the soil redistribution induced SOC fluxes at the catchment scale.

*Acknowledgements*—The study was carried out in the framework of the German Research Foundation (DFG) project 'Soil redistribution in agricultural landscapes – source or sink of $CO_2$?' FI 1216/4-1. Funding is gratefully acknowledged. Special thanks also go to the farm owner Mr Töllner for his permission to carry out several field campaigns and his patience in answering field management questions.

## REFERENCES

Aigner A. 1998. Zwischenfruchtbau. 11 495–500. In *Die Landwirtschaft 1. Pflanzliche Erzeugung*. BLV mbH: München.

Andrén O, Kätterer T. 1997. ICBM: the introductory carbon balance model for exploration of soil carbon balances. *Ecological Applications* **7**: 1226–1236.

Auerswald K. 2006. Germany. In *Soil Erosion in Europe*, Boardman J, Poesen J (eds). Wiley: Chichester; 213–230.

Berhe AA, Harte J, Harden JW, Torn MS. 2007. The significance of the erosion-induced terrestrial carbon sink. *BioScience* **57**: 337–346.

Beven K, Kirkby M. 1979. A physically based, variable contributing area model of basin hydrology. *Hydrological Sciences Bulletin* **24**: 43–69.

Billings SA, Buddemeier RW, Richter D, Van Oost K, Bohling G. 2010. A simple method for estimating the influence of eroding profiles on atmospheric $CO_2$. *Global Biogeochemical Cycles* **24**. DOI: 10.1029/2009 GB003560. 14 pp.

Ciais PM, Wattenbach M, Vuichard N, Smith P, Piao S, Don A, Luyssaert S, Janssens IA, Bondeau A, Dechow R, Leip A, Smith PC, Beer C, Van der Werf GR, Gervois S, Van Oost K, Tomelleri E, Freibauer A, Schulze ED. 2010. The European carbon balance. Part 2: croplands. *Global Change Biology* **16**: 1409–1428.

Desmet PJJ, Govers G. 1996a. A GIS procedure for automatically calculating the USLE LS factor on topographically complex landscape units. *Journal of Soil and Water Conservation* **51**: 427–433.

Desmet PJJ, Govers G. 1996b. Comparison of routing algorithms for digital elevation models and their implications for predicting ephemeral gullies. *International Journal of Geographic Information Systems* **10**: 311–331.

Desmet PJJ, Govers G. 1997. Two-dimensional modelling of the within-field variation in rill and gully geometry and location related to topography. *Catena* **29**: 283–306.

Deutsches Institut für Normung. 2002. *DIN ISO 11277: 2002–08 Bodenbeschaffenheit – Bestimmung der Partikelgrößenverteilung in Mineralböden – Verfahren mittels Siebung und Sedimentation*. Beuth Verlag: Berlin.

Deutsches Institut für Normung. 2005. *DIN 19708 – Bodenbeschaffenheit – Ermittlung der Erosionsgefährdung von Böden durch Wasser mit Hilfe der ABAG*. Beuth Verlag: Berlin.

Dlugoß V, Fiener P, Schneider K. 2010. Layer-specific analysis and spatial prediction of soil organic carbon using terrain attributes and erosion modeling. *Soil Science Society of America Journal* **74**: 922–935.

Draycott AP. 2006. *Sugar Beet*. Blackwell: Oxford.

Edwards WM, Owens LB. 1991. Large storm effects on total soil erosion. *Journal of Soil and Water Conservation* **46**: 75–78.

Eynard A, Schumacher TE, Lindstrom MJ, Malo DD. 2005. Effects of agricultural management systems on soil organic carbon in aggregates of Ustolls and Usterts. *Soil & Tillage Research* **81**: 253–263.

Fiener P, Auerswald K. 2003. Concept and effects of a multi-purpose grassed waterway. *Soil Use and Management* **19**: 65–72.

Fiener P, Auerswald K. 2007. Rotation effects of potato, maize and winter wheat on soil erosion by water. *Soil Science Society of America Journal* **71**: 1919–1925.

Fiener P, Dlugoß V, Korres W, Schneider K. 2011. Spatial variability of soil respiration in a small agricultural watershed – are patterns of soil redistribution important? *Catena*. DOI: 10.1016/j.catena.2011.05.014

Food and Agriculture Organization (FAO). 1998. *World Reference Base for Soil Resources*. United Nations: Rome.

Frede H-G, Dabbert S. 1999. *Handbuch zum Gewässerschutz in der Landwirtschaft*. Ecomed: Landsberg.

Gan YT, Campbell CA, Janzen HH, Lemke RL, Basnyat P, McDonald CL. 2009. Carbon input to soil from oilseed and pulse crops on the Canadian prairies. *Agriculture, Ecosystems & Environment* **132**: 290–297.

Govers G, Vandaele K, Desmet P, Poesen J, Bunte K. 1994. The role of tillage in soil redistribution on hillslopes. *European Journal of Soil Science* **45**: 469–478.

Grant DM, Dawson BD. 1997. *Isco Open Channel Flow Measurement Handbook*. Lincoln.

Gregorich EG, Greer KJ, Anderson DW, Liang BC. 1998. Carbon distribution and losses: erosion and deposition effects. *Soil & Tillage Research* **47**: 291–302.

Harden JW, Sharpe JM, Parton WJ, Ojima DS, Fries TL, Huntington TG, Dabney SM. 1999. Dynamic replacement and loss of soil carbon by eroding cropland. *Global Biogeochemical Cycles* **13**: 885–901.

Harkness DD, Harrison AF, Bacon PJ. 1986. The temporal distribution of 'bomb' $^{14}C$ in a forest soil. *Radiocarbon* **28**: 328–337.

Herbst M, Prolingheuer N, Graf A, Huisman JA, Weihermüller L, Vanderborght J. 2009. Characterization and understanding of bare soil respiration spatial variability at plot scale. *Soil Science Society of America Journal* **8**: 762–771.

Hütsch BW, Augustin J, Merbach W. 2002. Plant rhizodeposition – an important source for carbon turnover in soils. *Journal of Plant Nutrition and Soil Science* **165**: 397–407.

Izaurralde RC, Williams JR, Post WM, Thomson AM, McGill WB, Owens LB, Lal R. 2007. Long-term modeling of soil C erosion and sequestration at the small watershed scale. *Climatic Change* **80**: 73–90.

Janzen HH. 2006. The soil carbon dilemma: shall we hoard it or use it? *Soil Biology and Biochemistry* **38**: 419–424.

Jarecki MK, Lal R, James R. 2005. Crop management effects on soil carbon sequestration on selected farmers' fields in northeastern Ohio. *Soil & Tillage Research* **81**: 265–276.

Kätterer T, Reichstein M, Andrén O, Lomander A. 1998. Temperature dependence of organic matter decomposition: a critical review using literature data analyzed with different models. *Biology and Fertility of Soils* **27**: 258–262.

Kilpatrick FA, Schneider VR. 1983. *Use of Flumes in Measuring Discharge*. United States Government Printing Office: Washington, DC.

Lal R. 2003. Soil erosion and the global carbon budget. *Environment International* **29**: 437–450.

Levin I, Kromer B. 2004. The tropospheric $^{14}CO_2$ level in mid-latitudes of the northern hemisphere (1959–2003). *Radiocarbon* **46**: 1261–1272.

Li S, Lobb DA, Tiessen KHD, McConkey BG. 2010. Selecting and applying Cesium-137 conversion models to estimate soil erosion rates in cultivated fields. *Journal of Environmental Quality* **39**: 204–219.

Lindstrom MJ, Nelson WW, Schumacher TE. 1992. Quantifying tillage erosion rates due to moldboard plowing. *Soil & Tillage Research* **24**: 243–255.

Liu S, Bliss N, Sundquist E, Huntington TG. 2003. Modeling carbon dynamics in vegetation and soil under the impact of soil erosion and deposition. *Global Biogeochemical Cycles* **17**: 1074.

Ludwig B, Schulz E, Rethemeyer J, Merbach I, Flessa H. 2007. Predictive modelling of C dynamics in the long-term fertilization experiment at Bad Lauchstädt with the Rothamsted Carbon Model. *European Journal of Soil Science* **58**: 1155–1163.

McCool DK, Brown LC, Foster GR, Mutchler CK, Meyer LD. 1987. Revised slope steepness factor for the Universal Soil Loss Equation. *Transactions of the American Society of Agricultural Engineers* **30**: 1387–1396.

Nash JE, Sutcliffe JV. 1970. River flow forecasting through conceptual models: Part I. A discussion of principles. *Journal of Hydrology* **10**: 282–290.

Parton WJ, Schimel DS, Cole CV, Ojima DS. 1987. Analysis of factors controlling soil organic matter levels in Great Plains grasslands. *Soil Science Society of America Journal* **51**: 1173–1179.

Pennock DJ, Frick AH. 2001. The role of field studies in landscape-scale applications of process models: an example of soil redistribution and soil organic carbon modelling using CENTURY. *Soil & Tillage Research* **58**: 183–191.

Poesen JWA, Verstraeten G, Soenens R, Seynaeve L. 2001. Soil losses due to harvesting of chicory roots and sugar beet: an underrated geomorphic process? *Catena* **43**: 35–47.

Polyakov V, Lal R. 2004. Modeling soil organic matter dynamics as affected by soil water erosion. *Environment International* **30**: 547–556.

Preston N. 2001. Geomorphic Response to Environmental Change: The Imprint of Deforestation and Agricultural Land Use on the Contemporary Landscape of the Pleiser Hügelland, Bonn, Germany. PhD Thesis, Rheinische Friedrich-Wilhelms-Universität, Bonn.

Renard KG, Foster GR, Weesies GA, McCool DK, Yoder DC. 1996. *Predicting Soil Erosion by Water: A Guide to Conservation Planning with the Revised Universal Soil Loss Equation (RUSLE).* USDA-ARS: Washington, DC.

Renschler CS. 2003. Designing geo-spatial interfaces to scale process models: the GeoWEPP approach. *Hydrological Processes* **17**: 1005–1017.

Renwick WH, Smith SV, Sleezer RO, Buddemeier RW. 2004. Comment on 'Managing soil carbon' (II). *Science* **305**: 1567.

Rethemeyer J, Kramer C, Gleixner G, John B, Yamashita T, Flessa H, Andersen N, Nadeau MJ, Grootes PM. 2005. Transformation of organic matter in agricultural soils: radiocarbon concentration versus soil depth. *Geoderma* **128**: 94–105.

Ritchie JC, McCarty GW, Venteris ER, Kaspar TC. 2007. Soil and soil organic carbon redistribution on the landscape. *Geomorphology* **89**: 163–171.

Rosenbloom NA, Doney SC, Schimel DS. 2001. Geomorphic evolution of soil texture and organic matter in eroding landscapes. *Global Biogeochemical Cycles* **15**: 365–381.

Ruysschaert G, Poesen J, Verstraeten G, Govers G. 2004. Soil loss due to crop harvesting: significance and determining factors. *Progress in Physical Geography* **4**: 467–501.

Ruysschaert G, Poesen J, Verstraeten G, Govers G. 2005. Interannual variation of soil losses due to sugar beet harvesting in West Europe. *Agriculture, Ecosystems & Environment* **107**: 317–329.

Schlesinger WH. 2005. The global carbon cycle and climate change. *Advances in the Economics of Environmental Resources* **5**: 31–53.

Schwertmann U, Vogl W, Kainz M. 1987. *Bodenerosion durch Wasser – Vorhersage des Abtrags und Bewertung von Gegenmaßnahmen.* Ulmer Verlag: Stuttgart.

Smith SV, Renwick WH, Buddemeier RW, Crossland CJ. 2001. Budgets of soil erosion and deposition for sediments and sedimentary organic carbon across the conterminous United States. *Global Biogeochemical Cycles* **15**: 697–707.

Smith SV, Sleezer RO, Renwick WH, Buddemeier RW. 2005. Fates of eroded soil organic carbon: Mississippi basin case study. *Ecological Applications* **15**: 1929–1940.

Souchère V, King D, Daroussin J, Papy F, Capillon A. 1998. Effects of tillage on runoff directions: consequences on runoff contributing area within agricultural catchments. *Journal of Hydrology* **206**: 256–267.

Stallard R. 1998. Terrestrial sedimentation and the carbon cycle: coupling weathering and erosion to carbon burial. *Global Biogeochemical Cycles* **12**: 231–257.

Stuiver M, Polach HA. 1977. Discussion reporting of $^{14}C$ data. *Radiocarbon* **19**: 355–363.

Takken I, Beuselinck L, Nachtergaele J, Govers G, Poesen J, Degraer G. 1999. Spatial evaluation of a physically-based distributed erosion model (LISEM). *Catena* **37**: 431–477.

Takken I, Govers G, Steegen A, Nachtergaele J, Guerif J. 2001. The prediction of runoff flow directions on tilled fields. *Journal of Hydrology* **248**: 1–13.

Trumbore S. 2009. Radiocarbon and soil carbon dynamics. *Annual Review of Earth and Planetary Sciences* **37**: 47–66.

Van Hemelryck H, Fiener P, Van Oost K, Govers G. 2010. The effect of soil redistribution on soil organic carbon: an experimental study. *Biogeosience* **7**: 3971–3986.

Van Oost K, Govers G. 2006. Tillage erosion. In *Soil Erosion in Europe*, Boardman J, Poesen J (eds). Wiley: Chichester; 599–608.

Van Oost K, Govers G, Desmet P. 2000. Evaluating the effects of changes in landscape structure on soil erosion by water and tillage. *Landscape Ecology* **15**: 577–589.

Van Oost K, Govers G, Quine T, Heckarth G, Olesen JE, De Gryze S, Merckx R. 2005a. Landscape-scale modeling of carbon cycling under the impact of soil redistribution: the role of tillage erosion. *Global Biogeochemical Cycles* **19**: GB4014.

Van Oost K, Govers G, Van Muysen W. 2003. A process-based conversion model for caesium-137 derived erosion rates on agricultural land: an integrated spatial approach. *Earth Surface Processes and Landforms* **28**: 187–207.

Van Oost K, Quine TA, Govers G, De Gryze S, Six J, Harden JW, Ritchie JC, McCarty GW, Heckrath G, Kosmas C, Giraldez JV, Marques da Silva JR, Merckx R. 2007. The impact of agricultural soil erosion on the global carbon cycle. *Science* **318**: 626–629.

Van Oost K, Quine T, Govers G, Heckrath G. 2005b. Modeling soil erosion induced carbon fluxes between soil and atmosphere on agricultural land using SPEROS-C. 37–51. In *Advances in Soil Science. Soil Erosion and Carbon Dynamics,* Roose EJ, Lal R, Feller C, Barthes B, Stewart BA (eds). CRC Press: Boca Raton, FL.

Van Oost K, Van Hemelryck H, Harden JW. 2009. Erosion of soil organic carbon: implications for carbon sequestration. 189–202. In *Carbon Sequestration and its Role in the Global Carbon Cycle,* McPherson BJ, Sundquist ET (eds). American Geophysical Union: Washington, DC; 189–202.

Van Rompaey AJJ, Verstraeten G, Van Oost K, Govers G, Poesen J. 2001. Modelling mean annual sediment yield using a distributed approach. *Earth Surface Processes and Landforms* **26**: 1221–1236.

Verstraeten G, Poesen J, Gillijns K, Govers G. 2006. The use of riparian vegetated filter strips to reduce river sediment loads: an overestimated control measure? *Hydrological Processes* **20**: 4259–4267.

Walling DE, He Q, Whelan PA. 2003. Using $^{137}CS$ measurements to validate the application of the AGNPS and ANSWERS erosion and sediment yield models in two small Devon catchments. *Soil & Tillage Research* **69**: 27–43.

Wang Z, Govers G, Steegen A, Clymans W, Van den Putte A, Langhans C, Merckx R, Van Oost K. 2010. Catchment-scale carbon redistribution and delivery by water erosion in an intensively cultivated area. *Geomorphology* **124**: 65–74.

Wischmeier WH, Smith DD. 1978. *Predicting rainfall erosion losses – a guide to conservation planning.* United States Government Printing Office: Washington, DC.

Yadav V, Malanson GP. 2009. Modeling impacts of erosion and deposition on soil organic carbon in the Big Creek Basin of southern Illinois. *Geomorphology* **106**: 304–314.

Yoo K, Amundson R, Heimsath AM, Dietrich WE. 2005. Erosion of upland hillslope soil organic carbon: coupling field measurements with a sediment transport model. *Global Biogeochemical Cycles* **19**: GB3003.